

Synthesis, Crystal Structures, and Ion Pairing of κ^6N Complexes with Rare-Earth Elements in the Solid State and in Solution

Perrine M. R. Wingerling,^[a] Silvia Hohnstein,^[a] Felix Krämer,^[a] Melina E. A. Dilanas,^[a] Cristina Ruiz-Martínez,^[b] Ignacio Fernández,^{*[b]} and Frank Breher^{*[a]}

The rare earth element complexes (Ln=Y, La, Sm, Lu, Ce) of several podant κ^6N -coordinating ligands have been synthesized and thoroughly characterized. The structural properties of the complexes have been investigated by X-ray diffraction in the solid state and by advanced NMR methods in solution. To estimate the donor capabilities of the presented ligands, an experimental comparison study has been conducted by cyclic voltammetry as well as absorption experiments using the

cerium complexes and by analyzing ^{89}Y NMR chemical shifts of the different yttrium complexes. In order to obtain a complete and detailed picture, all experiments were corroborated by state-of-the-art quantum chemical calculations. Finally, coordination competition studies have been carried out by means of 1H and ^{31}P NMR spectroscopy to investigate the correlation with donor properties and selectivity.

Introduction

The coordination chemistry of the trivalent f-block elements is very diverse^[1] and lanthanide(III) ions are classified as hard Lewis acids relating to the HSAB (hard/soft Lewis-acid/base) theory.^[2] Considering this, the Ln^{3+} ions show a high coordination affinity with hard electron donating groups such as oxygen or fluorine.^[3]

For a long time, *N*-donor ligands were considered to be too soft for the complexation with lanthanide cations. Meanwhile, multiple rare earth elements (REE) were coordinated with nitrogen-based ligands such as amine,^[4] guanidine,^[5,6] *N*-heterocycles^[7] or Schiff bases,^[8] evidencing technological and scientific applications in catalysis,^[5,9] medicine,^[10] luminescent materials,^[11] or in magnetochemistry.^[12] Another application, in which tri-^[13] and tetradentate^[14] nitrogen-based ligands have shown effectiveness, is for the nuclear waste treatment.

Nuclear waste treatment is of important interest because 10.000 tons have to be safely disposed per year.^[15] The nuclear

waste is composed of highly radioactive compounds such as uranium, plutonium and minor actinides americium, curium, neptunium and their long-lived fission products.^[16] Radioactive waste represents a risk for human and environmental health^[17] and the proper disposal of the waste is essential. Therefore, the Advanced Fuel Cycle (AFC) has been developed and is attractive: in addition to decreasing the waste volume, it simplifies the requirements for a repository due to the low long-term risk potential.^[18] According to this method, highly radioactive nuclear waste is separated (Partitioning) and the minor actinides are transformed into stable fission products or rather to nuclides with a short half-life time (Transmutation). After separation of uranium, plutonium and neptunium by the PUREX process,^[19] americium(III), curium(III) and the lanthanides are isolated from the other fission products using the DIAMEX process.^[20] Finally, the SANEX process allows the separation of Am(III) and Cm(III) from the lanthanides using *N*-donor ligands, for example, containing bis-triazinyl-pyridine (BTP) or bis-triazinyl-bipyridine (BTBP) moieties (see Scheme 1).^[21] The transmutation of Am(III) and Cm(III) is made by reaction with neutrons^[22] and some lanthanides show a high neutron absorption ratio that drastically decrease the efficiency of the reaction. For this reason, the separation of the lanthanides from the Am(III) and Cm(III) is imperative to improve the transmutation yield. However, the separation of 4f- and 5f-elements is challenging because of their chemical similarities, and therefore investigation of their coordination chemistry will help to better understand which properties are decisive for selective coordination.^[23] Sterics, the bond lengths to the actinide, or stoichiometry involved between the ligand and the metal are the most discussed aspects that influence the ligand selectivity.^[24]

To better investigate the electronic and steric role of ligands in coordination with f-elements, the use of rigid tripodal ligands is of great interest. Our group already reported a κ^6N donor

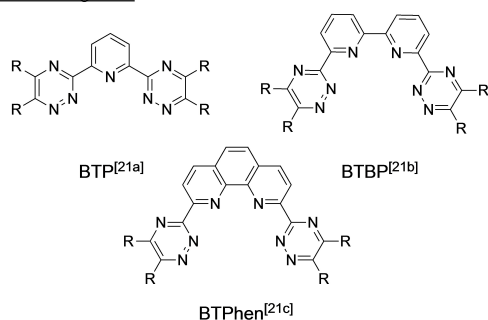
[a] P. M. R. Wingerling, Dr. S. Hohnstein, Dr. F. Krämer, M. E. A. Dilanas, Prof. Dr. F. Breher
Institute of Inorganic Chemistry
Karlsruhe Institute of Technology (KIT)
Engesserstr. 15, 76131 Karlsruhe (Germany)
E-mail: breher@kit.edu

[b] Dr. C. Ruiz-Martínez, Prof. Dr. I. Fernández
Laboratory of Organic Chemistry
University of Almería Carretera de Sacramento s/n
04120 Almería (Spain)
E-mail: ifernan@ual.es

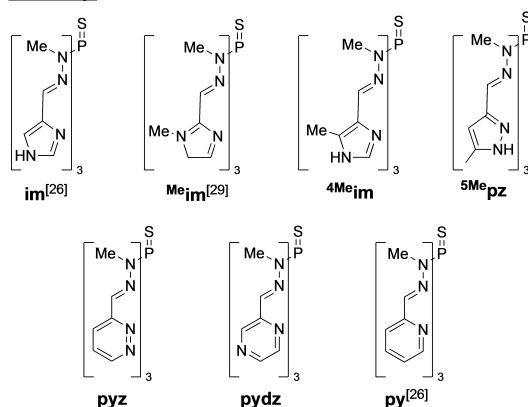
Supporting information for this article is available on the WWW under <https://doi.org/10.1002/chem.202301529>

© 2023 The Authors. Chemistry - A European Journal published by Wiley-VCH GmbH. This is an open access article under the terms of the Creative Commons Attribution License, which permits use, distribution and reproduction in any medium, provided the original work is properly cited.

Established ligands:



This study:



Scheme 1. Established polydentate *N*-donor ligands and $\kappa^6\text{N}$ donor ligands investigated in this study.

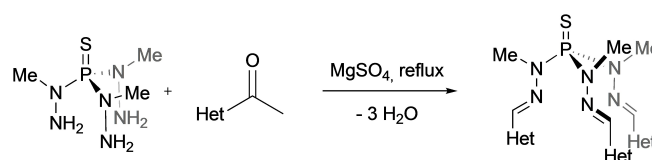
ligand that exhibits coordination ability with trivalent REE and plutonium.^[25] By using this ligand backbone and varying the *N*-heterocyclic substituents on the ligand donor entities, it was possible to synthesize multiple comparable ligand systems with varying electronic and steric properties (cf., Scheme 1).

We report herein the synthesis of various $\kappa^6\text{N}$ donor ligands and their complexation ability with several Ln^{3+} ions. Most of the compounds are characterized in detail using X-ray diffraction, pulsed field-gradient spin-echo (PGSE) diffusion NMR measurements, and low-temperature multinuclear NMR spectroscopy. The donating character of the ligands is investigated by complexation with cerium triflate followed by cyclic voltammetry, ⁸⁹Y NMR of the resulting yttrium complexes and UV-vis spectroscopy. All experiments were accompanied by quantum chemical calculations to shed more light on the donor capabilities. Finally, competition assays performed between ligands and lanthanide precursors examine the selectivity of the different ligands.

Results and Discussion

Synthesis

The synthesis of the $\kappa^6\text{N}$ donor ligands $(\text{S})\text{P}[\text{N}(\text{Me})\text{N}=\text{C}(\text{H})\text{-Het}]_3$ (Het = heterocycle: **im**, 1*H*-imidazolyl; **Meim**, *N*-methyl-1*H*-imidazolyl; **py**: pyridyl) have been previously reported by our group.^[26] Following similar reaction conditions, the synthesis of



Scheme 2. Synthesis of the ligands.

$(\text{S})\text{P}[\text{N}(\text{Me})\text{N}=\text{C}(\text{H})\text{-Het}]$ (Het: ⁴Me**im**: 4-methyl-1*H*-imidazolyl; ⁵Me**pz**: 5-methyl-1*H*-pyrazolyl; **pyz**: pyrazine; **pydz**: pyridazine) were performed by imine condensation between 1,1,1-trimethylthiophosphoryltrihydrazide ($\text{SP}(\text{NMe-NH}_2)_3$) and the corresponding carboxaldehydes of the heterocycles (Scheme 2).

The obtained ligands were recrystallized from acetonitrile, hexane/chloroform or cold ethanol (see Experimental Section). The formation of the ligands was verified by ¹H NMR spectroscopy by disappearance of the aldehyde signals ($\delta_{\text{H}}=9.5\text{--}10.5$ ppm) and by ³¹P NMR spectroscopy by shifting of the signal to lower frequencies ($\delta_{\text{P}}=72.3\text{--}72.9$ ppm) compared to $\text{SP}(\text{NMe-NH}_2)_3$.

Complexation experiments with $\text{Ln}(\text{OTf})_3$ ($\text{Ln}=\text{Y}$, La, Ce, Sm, Lu) were carried out in THF at room temperature under an atmosphere of argon. In all cases, complexes of the general formula $[(\kappa^6\text{N-L})\text{Ln}(\text{OTf})_3]$ were obtained, generally denoted as **M(Het)** hereafter, depending on the metal (M) and the heterocycle in the ligand $(\text{S})\text{P}[\text{N}(\text{Me})\text{N}=\text{C}(\text{H})\text{-Het}]_3$. The different lanthanides were chosen to investigate the coordination of the ligands with those of small (Y and Lu), middle (Sm), or large ionic radii (La). Cerium is redox-active and enables cyclic voltammetry measurements for experimental analysis of the donor properties of the ligands.^[27] Unfortunately, no pure products were obtained by complexation of different lanthanide triflates with **pyz** and **pydz**. For the ligand **Meim**, only **Ce(Meim)** could be obtained in analytically pure form.

Solid state structures

The structures of all reported complexes are very similar, establishing $\kappa^6\text{N}$ mononuclear species (Figure 1). Selected bond lengths are summarized in Table 1. The cationic metal atoms are coordinated in each case by three triflate counter ions ($\kappa^1\text{O}$) and three imine and three heterocyclic nitrogen atoms ($\kappa^6\text{N}$) of the donor ligand. The only exception is observed for the **Lu(im)** complex, where one triflate counter-ion is not directly coordinated to the metal centre in the solid state. This behaviour can be explained by the smaller ionic radius of the Lu^{3+} cation compared to the other lanthanides (La^{3+} : 121.6 pm, Ce^{3+} : 119.6 pm, Y^{3+} : 107.5 pm and Lu^{3+} : 103.2 pm).^[28] Another structural difference is the coordination of the **im** ligand with cerium and lutetium. For lutetium, three imine nitrogen atoms N2, N4 and N6, and three imidazole nitrogen atoms N7, N9 and N11 are coordinated to the central atom. However, for the cerium complex, one *N*-Me (N2) nitrogen donor and only two N_{imine} donors (N4 and N6) are coordinated to the cerium centre.

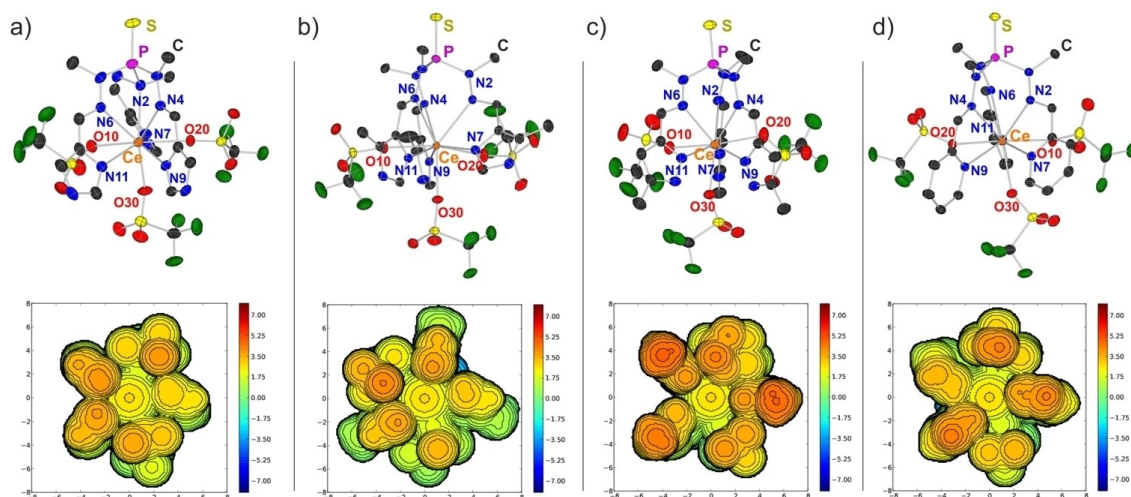


Figure 1. Solid-state molecular structures of the $[(\kappa^6N-L)Ce^{III}]$ complexes and the associated calculated steric maps using SambVca.^[30] Views are given from below omitting the lowest triflate anions (O30): **Ce(im)** (a), **Ce(^{4Me}im)** (b), **Ce(^{5Me}pz)** (c) and **Ce(py)** (d). Thermal ellipsoids are given at the 30% probability level. Hydrogen atoms are omitted for clarity.

Table 1. Selected bond lengths (Å).

	Lu(im)	Ce(im)	Ce(^{4Me} im)	Y(^{5Me} pz)	La(^{5Me} pz)	Ce(^{5Me} pz)	Ce(py)
M–N2	2.428(11)	2.743(5)	2.718(2)	2.711(3)	2.721(3)	2.692(3)	2.799(2)
M–N4	2.265(13)	2.666(5)	2.634(2)	2.568(3)	2.700(3)	2.752(3)	2.658(2)
M–N6	2.511(12)	2.707(5)	2.803(2)	2.582(3)	2.775(3)	2.696(2)	2.689(2)
M–N7	2.364(13)	2.612(6)	2.594(2)	2.457(3)	2.660(3)	2.554(3)	2.643(2)
M–N9	2.363(12)	2.579(5)	2.621(2)	2.444(3)	2.576(3)	2.550(3)	2.670(2)
M–N11	2.371(12)	2.623(6)	2.570(2)	2.478(3)	2.565(3)	2.639(3)	2.681(2)
M–O10	2.216(11)	2.469(4)	2.474(2)	2.324(3)	2.471(2)	2.443(2)	2.478(2)
M–O20	2.265(10)	2.462(5)	2.290(2)	2.367(3)	2.540(3)	2.495(3)	2.430(2)
M–O30		2.448(4)	2.479(2)	2.350(2)	2.466(2)	2.465(2)	2.477(2)

For the **M(im)** complexes (M=Lu, Ce), the Lu–N_{imine} (\varnothing 2.521 Å) and Lu–N_{im} (\varnothing 2.366 Å) bond lengths were found to be considerably shorter than the corresponding values detected for **Ce(im)**, i.e. Ce–N_{imine} (\varnothing 2.687 Å) and Ce–N_{im} (\varnothing 2.604 Å). This is also reflected in the M–O bond lengths of \varnothing 2.240 Å for Lu–O and \varnothing 2.460 Å for Ce–O, respectively.

For the **M(^{5Me}pz)** complexes, the M–N bond lengths of the La and Ce complexes are very similar, while those of **Y(^{5Me}pz)** are much shorter. Typical values are, for instance, Ce–N_{imine} (\varnothing 2.713 Å) and Ce–N_{pz} (\varnothing 2.579 Å) versus Y–N_{imine} (\varnothing 2.620 Å) and Y–N_{pz} (\varnothing 2.459 Å). The same trend is observed for the M–O bond lengths: while La–O and Ce–O are similar, the Y–O bonds are 0.145 Å shorter.

All cerium complexes shown in Figure 1 possess similar bond lengths (cf. Table 1).^[28] In order to quantify the steric profile and the ligand “pockets” of the κ^6N ligands **im**, **^{4Me}im**, **^{5Me}pz**, and **py**, we have analysed selected geometric measures for tris-bidentate ligands.^[29] It was of particular interest if the trigonal torsion and metal–ligand bond lengths are correlated in Ce complexes featuring different heteroatoms in the multi-dentate ligands (Figure 2 and Table 2). All the cerium complexes

Table 2. Selected structural details for the cerium complexes (cf. Figure 2).

	Ce(im)	Ce(^{4Me} im)	Ce(^{5Me} pz)	Ce(py)
$\varnothing d(\text{Ce}-N_{\text{imine}})/\text{Å}$	2.687 Å	2.718	2.713 Å	2.715
$\varnothing d(\text{Ce}-N_{\text{het}})/\text{Å}$	2.604 Å	2.595	2.579 Å	2.664
$h_1^{[a]}/\text{Å}$	2.565	2.593	2.630	2.552
$h_1^{[b]}/\text{Å}$	2.141	2.057	2.017	2.033
$h_2^{[b]}/\text{Å}$	0.464	0.528	0.618	0.505
$bite^{[a]}/\text{Å}$	2.825	2.778	2.758	2.756
$d^{[a]}/\text{Å}$	2.862	3.050	3.115	2.083
$c^{[a]}/\text{Å}$	4.253	4.248	4.186	4.349
$\vartheta^{[a]}/^\circ$	65.267	62.972	62.729	61.607

[a] according to Figure 2; [b] h_1 and h_2 denote the distance of the central metal ion from the planes defined by $(N_{\text{imine}})_3$ and $(N_{\text{het}})_3$, respectively.

show comparable geometrical structures. However, **Ce(im)** stands out from the crowd with a larger θ angle and longer *bite* distances compared to the other complexes. The $d(\text{Ce}-N_{\text{imine}})$ bonds are shorter for **Ce(im)** although the h_2 distance is the shortest, which confirms the higher distortion expressed by θ .

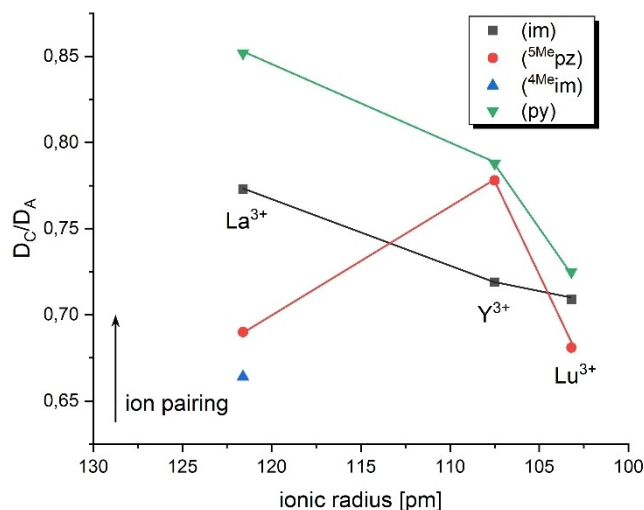


Figure 3. Variation of the ratio D_C/D_A as a function of ionic radius (in pm) of the central metal ion in CD_3CN at 292 K (D_C/D_A = quotient of the diffusion coefficient of cationic and anionic species, $c = 30$ mM).

The cationic hydrodynamic radii (r_H) of the **im**-based complexes are in the range of $r_H = 5.9$ – 6.2 Å, while the determined anionic hydrodynamic radii are about 1.6 Å smaller than the cationic species. Based on the quotient of cationic (D_C) and anionic (D_A) diffusion coefficients, the grade of ion pairing can be determined. For the $D_C/D_A = 1$ value, all triflate counterions would be fully coordinated, a deviation from the unity value is an indication for some degree of solvent separated ion pairs (SSIPs) and therefore the non-coordination of the triflate species to some extent is evident. As shown in Table 3, all complexes are SSIPs in solution. Regarding the **im**-based complexes, the La complexes exhibit the highest D_C/D_A value, followed by the yttrium and then lutetium complexes, which are well-correlated to the decreasing ionic radii. For **Lu(im)**, the D_C/D_A value is comparable with the one reported previously for **Lu(py)** ($D_C/D_A = 0.725$,^[25] cf. **Lu(im)**: $D_C/D_A = 0.709$). The lanthanum complex with the **py** ligand **Ln(py)** follows the same tendency, that is, a reduction of the diffusion ratio D_C/D_A within the ionic radius (Figure 3). The complex **La(py)** exhibits a much higher D_C/D_A value ($D_C/D_A = 0.877$ ^[25]) as compared to **La(im)** ($D_C/D_A = 0.773$) and compared to **Y(py)** and **Lu(py)**. Another difference between **py** and **im** is the increased ion pairing in the La and the Y complexes and much reduced increment in the Lu complex. A smaller ligand ‘pocket’ of the latter, compared to **py**, which shows a more conical geometry, is a possible explanation for this difference. As observed in the previous section, in the X-ray structure of **Ce(im)**, three triflate counterions were coordinated to the cerium centre. Instead, in **Lu(im)**, the third triflate ion is dissociated from the metal centre. The larger ionic radius of cerium enables the coordination of three anions but by decreasing the ionic radius, there is just enough space for two counter-ions to coordinate to the lutetium centre. As discussed above, the **im** ligand displays a high distortion by coordination of cerium, which is not enough to coordinate with the lutetium centre and three further triflate counterions. When **5Me_pz** is involved, the linear decreasing tendency is broken, with the yttrium complex showing

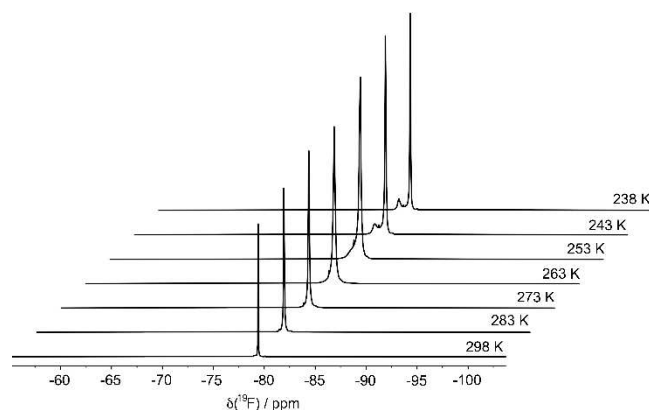


Figure 4. ^{19}F NMR (282.40 MHz, CD_3CN) spectra of **Y(im)** as a function of temperature in acetonitrile.

a higher D_C/D_A quotient than the La complex, the former of smaller ionic radius. In this sense, **La(5Me_pz)** and **Lu(5Me_pz)** display very small D_C/D_A values compared to **Y(5Me_pz)**. For **Y(5Me_pz)**, the quotient is comparable to that of **Y(py)** and is higher than the value of **La(im)**. Related to this, the D_C/D_A quotient of **La(4Me_im)** is also very low and not comparable to the others obtained for **La(im)** and **La(py)**. The D_C/D_A values obtained for the different lanthanum complexes confirm the statement done by analysis of the steric maps. The ligands **4Me_im** and **5Me_pz** crowd the metal center, which results in the coordination of the third triflate anion being complicated and consequently the D_C/D_A values being smaller than for **im** and **py**.

Low Temperature ^{19}F NMR Spectroscopy

As mentioned in the previous paragraph, the triflate groups are partially dissociated from the Ln centre in solution. For **Lu(im)**, a dissociated triflate group is observed in the solid state. However, only one signal is observed by the ^{19}F NMR spectroscopy experiment at room temperature in acetonitrile, supporting the view of a fast exchange at room temperature. To further investigate the dissociation of the triflate group, ^{19}F NMR spectroscopy measurements of **Y(im)** and **Lu(im)** at lower temperature were performed. At low temperature, the exchange between the associated and dissociated form of the triflate group is slowed down and two ^{19}F NMR signals are observed as previously reported.^[25]

For **Y(im)**, a broadening of the signal at $\delta_F = -79.4$ ppm is observed by lowering the temperature to 253 K, followed by splitting into two signals at 243 K (Figure 4). The one at lowest chemical shift is reasonably sharp ($W_{1/2} = 17.4$ Hz), and the one at higher frequency significantly broad ($W_{1/2} = 44.3$ Hz) due to a probably non-resolved exchange between two of the three triflate anions.

As mentioned previously, PGSE NMR experiments indicated a smaller ion pairing for **Lu(im)** than for **Y(im)**, and therefore the same low temperature NMR experiments were performed with **Lu(im)** to look for similarities. However, no signal splitting was observed by lowering the temperature to 233 K and only a

much broader signal was evidenced (Figure S97). The low temperature NMR measurements were done in acetonitrile, which freezes at 228 K. Therefore, measurements at lower temperatures were not possible. The use of other deuterated solvents such as acetone ($T_m = 178$ K) or THF ($T_m = 165$ K) could not be employed due to the low solubility of the complexes in these solvents.

⁸⁹Y NMR spectroscopy

⁸⁹Yttrium NMR measurements were performed to investigate the donor character of the different ligand systems. Faster measurements are obtained when using indirect methods, and therefore two-dimensional ¹H, ⁸⁹Y HMBC NMR experiments were performed to unravel their chemical shifts (see Supporting Information). The ⁸⁹Y nucleus showed a scalar interaction with the imine proton of the different complexes. The yttrium chemical shifts were all located in the range from $\delta_Y = -17.8$ to $+56.6$ ppm, and are clearly distinct among the different complexes. Although a correlation between the ⁸⁹Y chemical shifts and the metal coordination number is unclear,^[36] there are examples in which the signal is located at lower chemical shifts when strong donor atoms surround the nucleus with a higher coordination number. Table 4 shows the experimental ⁸⁹Y NMR chemical shifts for the complexes under study. Interestingly, imidazole-like ligands (⁴Meim, ^{Me}im, and im) showed positive chemical shifts, while **py**- and **pz**-like ligands showed negative chemical shifts. **Y**(⁵Me**pz**) exhibits the lowest chemical shift of $\delta_Y = -17.8$ ppm followed by **Y**(**py**) with a signal at $\delta_Y = -4.9$ ppm. The substitution patterns in the imidazole ring and the strength of the nitrogen bonding to the yttrium atom seem to play an important role in driving the ion pairing capabilities. In this sense, the **Y**(⁴Meim) complex has the

highest chemical shift of the entire series with a value of $\delta_Y = +56.6$ ppm, whereas the **Y**(^{Me}im) complex shows a more shielded signal at $\delta_Y = +17.9$ ppm.

At first glance, the observed trends seem to correlate well with the ion pairing features. For instance, the ⁴Meim-based ligand shows the smallest ion-pairing of the lanthanum complexes (smallest D_C/D_A value of 0.664) and is the one showing the highest yttrium chemical shift of $\delta_Y = +56.6$ ppm. In the yttrium series, a similar trend is observed. The im ligand shows the lowest ion pairing ratio and the highest yttrium chemical shift of $\delta_Y = +24.8$ ppm. In the case of **py** and ⁵Me**pz** ligands, both showed high D_C/D_A ratios, and both display negative chemical shifts of $\delta_Y = -17.8$ and -4.9 ppm, respectively. Although the dataset is very small at this stage, this could be a good probe to study the donor abilities within this series. To shed light on the coordination sphere of the Y atom in solution, the ⁸⁹Y NMR shifts of the complexes with three OTf groups as well as the cationic complexes where one OTf group is replaced by one MeCN (denoted as **[M(Het)-OTf]⁺** in Table 3) were calculated by means of DFT on TPSSh(B3LYP)/SARC-ZORA/TZVP level of theory including CPCM(MeCN) solvation correction (further details in the Supporting Information). The error of this method is about 20 ppm, which allows no exact determination of the coordination sphere in solution.^[37] Nevertheless, the cationic species clearly show a calculated ⁸⁹Y NMR chemical shift at lower field, which would be in line with the high chemical shift observed for **Y**(⁴Meim).

DFT Calculations

As already mentioned, we computed (TPSSh/QZVPP/D3BJ) the proton affinities (PA) and the energies of the donor orbitals of the isolated ligand *N*-donor entities. The results are given in Table 5 and Figure 5.

Not for all ligand entities the HOMO is the corresponding donor orbital (see caption of Figure 5 for details). The computed PA shows values between 1005–1051 kJ/mol. For the im-, ^{Me}im-, ⁴Meim-, ⁵Me**pz**- and **py**-based ligands, the calculated PA correlates well with the energies of the corresponding donor orbital such that with increasing orbital energies the PA increases as well. For the six-membered donors **pydz** and **pyz**, however, a reverse

Table 4. Experimental and computed ⁸⁹Y NMR chemical shifts.

	⁸⁹ Y NMR/ppm Experiment ^[b]	⁸⁹ Y NMR/ppm Method 1 ^[c]	⁸⁹ Y NMR/ppm Method 2 ^[d]
Y (im)	24.8	9.03	2.63
[Y (im)-OTf] ^{+[a]}	–	38.83	32.77
Y (^{Me} im)	17.9	22.80	18.24
[Y (^{Me} im)-OTf] ^{+[a]}	–	42.19	37.94
Y (⁴ Meim)	56.6	14.09	8.92
[Y (⁴ Meim)-OTf] ^{+[a]}	–	33.90	28.35
Y (⁵ Me pz)	–17.8	26.60	21.04
[Y (⁵ Me pz)-OTf] ^{+[a]}	–	32.54	27.92
Y (pydz)	–	22.07	11.75
[Y (pydz)-OTf] ^{+[a]}	–	44.11	34.89
Y (pyz)	–	38.96	30.94
[Y (pyz)-OTf] ^{+[a]}	–	48.40	41.12
Y (py)	–4.9	49.00	40.94
[Y (py)-OTf] ^{+[a]}	–	69.87	62.68

[a] Complexes with two coordinated triflates and one acetonitrile; [b] CD₃CN; [c] TPSSh/SARC-ZORA-TZVP; [d] B3LYP/SARC-ZORA-TZVP.

Table 5. Computed (TPSSh/QZVPP/D3BJ) donor orbital energies and proton affinities (PA).

	PA/kJ/mol	$E_{\text{donor orbital}}$ /eV	donor orbital
im	1021	–6.56	HOMO-1
^{Me} im	1051	–6.52	HOMO-1
⁴ Meim	1035	–6.49	HOMO-2
⁵ Me pz	1005	–6.67	HOMO-2
pydz	1027	–5.64	HOMO
pyz ^[a]	1018	–6.02	HOMO-1
py	1032	–6.26	HOMO-1

[a] Transition state with one imaginary frequency.

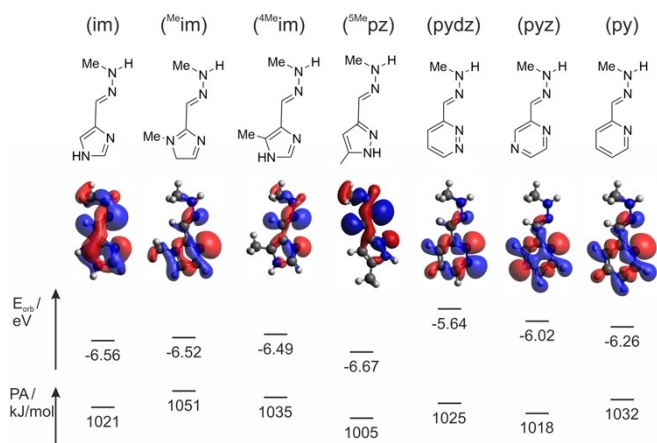


Figure 5. Plotted (iso = 0.02) donor orbitals (im: HOMO-1; ^{Me}im: HOMO-1; ^{4Me}im: HOMO-2; ^{5Me}pz: HOMO; pydz: HOMO-1; pyz: HOMO-1; py: HOMO-2), energies of the donor orbitals and proton affinity of the isolated ligand arms of im-py.

Electrochemistry

As mentioned in the introduction, the donor ability of the ligands can be determined by the oxidation potential of the Ce^{III}/Ce^{IV} redox couple of the corresponding Ce³⁺ complexes using cyclic voltammetry. Only a few cyclic voltammetry experiments of Ce^{III}/Ce^{IV} with polydentate N-donor ligands have been reported so far.^[38,39] Therefore, an additional [Ce(terpy)₂(OTf)₃] complex has been synthesized following the published procedure and the electrochemical behaviour has been investigated.^[40] The obtained cyclic voltammograms are shown in Section S4 of the Supporting Information. The measured oxidation and reduction potentials are summarized in Table 6. All complexes display irreversible oxidation and reduction waves, which attest for a high ligand reorganisation or slow electron transfer processes during the oxidation and/or reduction events. The difference between oxidation and reduction

Table 6. Measured first oxidation and reduction potentials of the synthesized cerium complexes in acetonitrile vs Fc/Fc⁺ (internal standard Fc/Fc⁺; conditions: Pt/[NBu₄][PF₆]/Ag; ν = 100 and 250 mV/s).

Compound	E_{ox}/V	$I_{pa}/\mu\text{A}$	E_{red}/V	$I_{pc}/\mu\text{A}$	$E_{ox}-E_{red}/\text{V}$
Ce(im)	100 mV/s	0.11	-1.01	0.56	2.45
	250 mV/s	1.47	-1.02	1.08	2.49
Ce(^{Me}im)	100 mV/s	1.16	-1.19	3.42	1.71
	250 mV/s	0.95	-1.25	5.26	1.72
Ce(^{4Me}im)	100 mV/s	0.16	-1.25	0.14	1.01
	250 mV/s	0.63	-1.24	0.27	0.98
Ce(^{5Me}pz)	100 mV/s	1.47	-1.78	0.66	3.45
	250 mV/s	1.67	-1.76	0.78	3.43
Ce(py)	100 mV/s	-	-1.26	3.16	-
	250 mV/s	1.08	-1.28	4.15	2.36
Ce(terpy)₂	100 mV/s	0.22	-1.01	0.10	2.72
	250 mV/s	1.71	-1.10	0.31	2.81

trend is observed. Taking the proton affinities into account, the following order of the donor strength results:



Following the energies of the corresponding donor orbitals (assuming the highest energy correlates with the strongest donor abilities), the order is:



This is due to the above-mentioned reverse trend in the PA and orbital energies of pydz and pyz.

potentials is varying to a great extent. **Ce(^{4Me}im)** displays the smallest difference between oxidation and reduction potential ($E_{ox} < E_{red} = 0.99$ V), followed by **Ce(^{Me}im)** with a comparable difference (1.71 V), as reported for the tridentate terpyridyl ligand before.^[38]

For almost all complexes, the reduction wave is more intense than the oxidation wave, which is in concordance with the reported results.^[38] The only observed exceptions occur for the **Ce(^{5Me}pz)** and **Ce(terpy)₂(OTf)₃** complexes. As mentioned above, the oxidation potential can be a gauge for the donor ability of the ligands. Indeed, the Ce⁴⁺ ion produced by oxidation should be more stabilized by a ligand with more donating character and the oxidation potential should be lower. Because of the very low intensity of the oxidation waves, DFT calculations have been performed to confirm the experimental results; for completeness reasons, **Ce(pydz)** and **Ce(pyz)** have

Complex ^[a]	E_{ion} (gas)	E_{HOMO} /eV (gas)	$E_{1/2}$ /V	$E_{1/2}$ /V (MeCN)
Ce(im)	593.72	-3.7074	4.97	0.31
Ce ^{(Me)im}	593.53	-3.8721	4.97	0.31
Ce ^{(4Me)im}	576.49	-3.5788	4.77	0.11
Ce ^{(5Me)pz}	607.84	-3.9251	5.09	0.43
Ce(pydz)	588.69	-4.1314	4.97	0.31
Ce(py)	644.03	-4.4391	5.21	0.55
Ce(py)	615.25	-4.1304	5.09	0.43

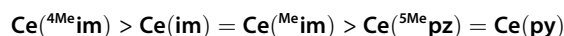
[a] Ce complexes including three OTf ligands.

also been calculated. For comparison with the experimental values, the first ionization energies, the HOMO energies (which can be correlated with the experimental redox potential),^[41] the half wave potentials $E_{1/2}$ and the half wave potentials vs Fc/Fc⁺ including CPCM(MeCN) solvation effects were calculated on the TPSS/TZVP level of theory including D3BJ dispersion correction. The results are summarized in Table 7.

The experimental and calculated oxidation potentials are not in agreement, which, however, is not surprising. The experiments show irreversible oxidations whereas the half wave potentials $E_{1/2}$ of fully reversible oxidations are obtained by quantum chemical calculations. Additionally, the error of the calculated values is 200–300 mV.^[42] The calculated values in Table 7 only serve as a qualitative comparison of the complexes. For the experimental results, the order



with Ce^{(4Me)im} containing the strongest and Ce^{(5Me)pz} the weakest donor is obtained. For the calculation, the trend



is found, where Ce^{(4Me)im} displays the strongest donor character, which is in line with the experiments. The two trends differ somewhat, but in general they gave a similar picture especially for Ce^{(4Me)im} and Ce^{(Me)im}. Moreover, when these values are compared to the ones for the proton affinity for the isolated ligand entities, these two ligands are displaying the strongest donating character too. The results obtained experimentally and theoretically are thus satisfactory.

The cerium(III) complexes in our study are all paramagnetic. To investigate where the single electron is localized in the structure of the complexes, the spin density has been calculated on the TPSS/TZVP level of theory including D3BJ dispersion correction. A representation of the localization of the spin density is shown in Section 10, Figure S98 of the Supporting Information. The calculations display a localization of the spin density at the cerium atom, which supports the hypothesis that the first oxidation occurs at the Ce³⁺ atom.

UV-vis spectroscopy

To obtain additional information about the donating ability of the ligands, we measured the UV-vis spectra of the cerium complexes in MeCN at 298 K (Figure 6). Additionally, we performed computational investigations using TD-DFT at the TPSSh/TZVP level of theory, with incorporated solvent effects CPCM(MeCN). The calculated absorption maxima and corresponding energies were found to be in good agreement with

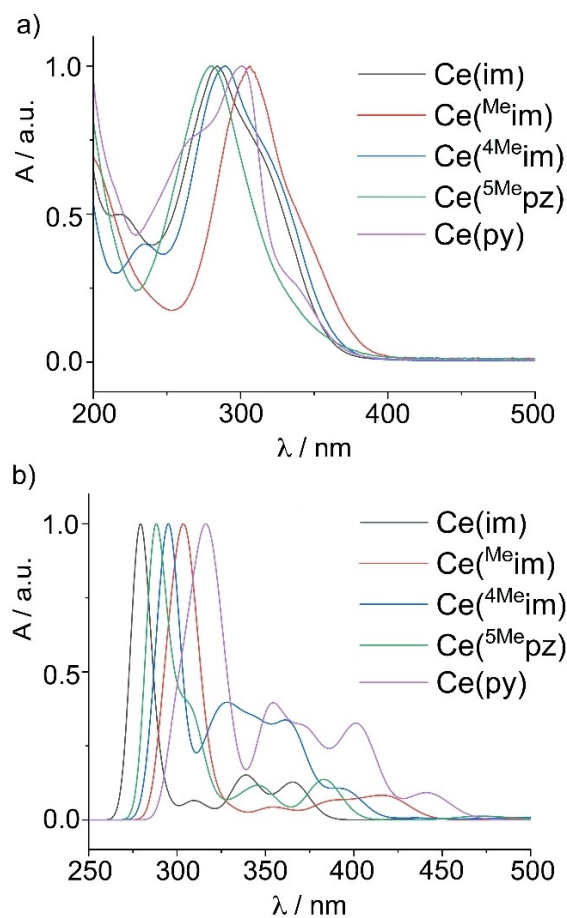


Figure 6. (a) Absorption spectra of Ce(im), Ce^{(Me)im}, Ce^{(4Me)im}, Ce^{(5Me)pz} and Ce(py) in MeCN at 298 K; (b) Computed UV-vis absorption spectra of in MeCN with three coordinated triflate counter ions.

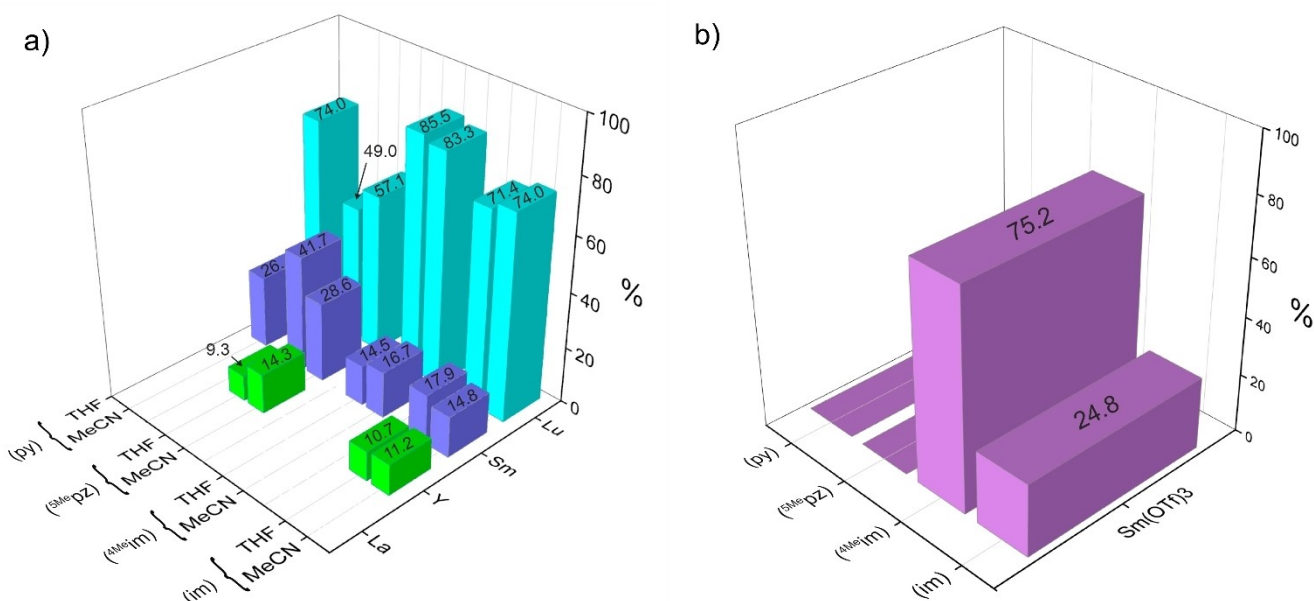


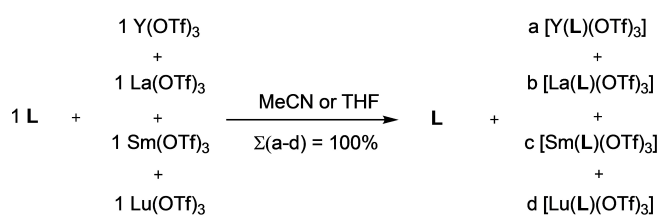
Figure 7. Results of the selectivity studies of (a) each ligand with the lanthanide precursors and (b) Sm(OTf)₃ with the different ligands im, ⁴Meim, ⁵Me-pz and py. Reaction solutions were stirred overnight at 298 K in MeCN or THF.

the experimental results. The energies obtained correspond to the HOMO–LUMO energy gap and primarily involve MLCT transitions. However, due to variations in the ligand-centred acceptor orbital that depend on the specific ligand used, we were unable to extract further information regarding the donor strengths from the UV-vis spectra.

Selectivity Studies

To investigate the selectivity of the different ligands, competition studies have been carried out by mixing one equivalent of a ligand with one equivalent of each lanthanide triflate precursors (Scheme 3). Due to the differing solubility of the complexes in THF, the studies were also carried out in acetonitrile where all complexes have approximately the same solubility.

After stirring overnight, ¹H and ³¹P NMR measurements of the reaction solutions were performed. To determine the proportion of each complex in solution, we analysed the obtained NMR spectra by integrating the detected signals. The value of the integrals when measured under quantitative



Scheme 3. Stoichiometric description of the competition reactions. L refers to im, ⁴Meim, ⁵Me-pz and py.

conditions (inverse-gated pulse sequence, 30° of pulse angle, and long recycle delays of 10s) gives the proportion of each complex in solution. The results are shown in Figure 7. For all ligands in both solvents, no formation of a La³⁺ complex is observed, and the most favoured complex is the Lu³⁺ complex. Since the ionic radius of La³⁺ (*r*_i = 121.6 pm)^[43] is larger than that of Lu³⁺ (*r*_i = 103.2 pm), the small cations apparently fit better in the ligand ‘pocket’ and its formation is favoured. However, a pure trend based on the ionic radii is not evident because the second most observed complexation is observed between the ligand and samarium triflate. The percentages of formation of the Sm³⁺ complexes ranges between 14.8% (with im in MeCN) and 41.7% (with ⁵Me-pz in THF). The yttrium complexes are formed in small amounts with the im- and ⁵Me-pz-based ligands, but no formation is observed with the ⁴Meim ligand. Complexation between py and Y(OTf)₃ is observed in THF, but the amount in solution could not be estimated. The most important finding was that the most selective ligand was the one which is based on ⁴Meim. In the competition experiment, Lu³⁺ is strongly preferred (83.3%) and only small amounts of the Sm³⁺ complex is formed (16.7%).

To provide further insight on the selectivity of the ⁴Meim-based ligand, additional competitiveness studies were carried out by mixing the different ligands im, ⁴Meim, ⁵Me-pz and py with one metal precursor. Unfortunately, the analysis of these results by ¹H and ³¹P NMR spectroscopy was found to be challenging. After the reaction, large amounts of free ligands remained in solution and generated NMR signals of high intensity. The identification of the ¹H and ³¹P NMR signals of the complexes were impossible using yttrium, lanthanum, or lutetium triflate and only the study with samarium triflate gave evaluable results. As shown in Figure 7, the ⁴Meim-based ligand is most selective within the series (75.2%), while other chelators such as

⁵Me₃pz and py showed no complexation. No conclusive results could be afforded in the case of the ⁴Meim-based ligand due to its very sparingly solubility. Since the electrochemical, computational, and also the NMR spectroscopic studies revealed the highest donating character for ⁴Meim within the series, this could be an explanation for the favored complexation with samarium.

Conclusions

Multiple REE complexes have been synthesized and characterized in the solid state and in solution. The X-ray single-crystal measurements attest to the structural similarities of the Ln complexes in the solid state. For all measured complexes, six nitrogen atoms of the podant κ⁶N-donor ligand and three triflate groups (κ¹O) are coordinated to the metal center. Only for Lu(im), a difference is observed, since the crystal structure shows one dissociated triflate group and one coordinated MeCN. The geometrical investigations and the steric maps suggest that im is the most flexible and py shows a conical geometry, which both enable the easier coordination of the third axial triflate counter-ion. The ion pairing of the different complexes was examined by PGSE-NMR spectroscopy, which supports the presence of dissociated OTf ligands in solution and enables the evaluation of the decreasing ion pairing with decreasing ionic radius for im and py. ⁴Meim and ⁵Me₃pz display lower ion pairing and support the obtained results by geometrical investigation and the steric maps. The donor character of the κ⁶N podant ligands has been investigated multidimensionally including state-of-the-art DFT and TD-DFT calculations as well as experimentally by cyclic voltammetry, ⁸⁹Y NMR spectroscopy and UV-Vis measurements. The computational and cyclic voltammetry studies revealed that the ⁴Meim-based κ⁶N chelate is the ligand with the most donating character. This was also supported by the NMR studies. Competition studies revealed that the ligands reported here favored the formation of lutetium complexes compared to those of the other lanthanide triflates. Lutetium is the lanthanide with the smallest ionic radius and apparently fits best into the ligands' coordination sphere. The competitiveness study between all the ligands and Sm³⁺ highlighted that the ⁴Meim-based ligand is the most favored one. Our laboratories are currently exploring the synthesis of novel, highly selective ligands to deepen our understanding of their behavior and facilitate their use in nuclear waste extraction processes. This research aims to enhance the effectiveness of these processes and contribute to the development of sustainable solutions for nuclear waste management.

Experimental Section

Computational details: All calculations have been performed with the ORCA 4.2^[44,45] or ORCA 5.0.3 program.^[44–46] Further details are given in the Supporting Information, Section S7.

General methods: All operations were carried out under dry argon using standard Schlenk and glovebox techniques. THF was freshly

distilled under argon from sodium/benzophenone, diethyl ether and diisopropyl ether from sodium–potassium alloy/benzophenone and acetonitrile from CaH₂ prior to use. CD₃CN was vacuum transferred from CaH₂ into thoroughly dried glassware equipped with Young Teflon valves. All chemicals were purchased from Aldrich or ABCR and used as received.

IR spectra were measured on a Bruker Alpha spectrometer using the attenuated reflection technique (ATR) and the data are quoted in wavelength numbers [cm⁻¹]. The intensity of the absorption band is indicated as vw (very weak), w (weak), m (medium), s (strong), vs. (very strong), and br (broad). Melting points were measured with a Thermo Fischer melting point apparatus and are not corrected. A Perkin–Elmer Lambda 9 UV/Vis spectrophotometer was used for recording absorption spectra at room temperature. Cyclic voltammetry measurements were performed with Gamry or Metrohm potentiostats and an electrochemical cell within a glovebox. We used a freshly polished Pt disk working electrode, a Pt wire as counter electrode, and a Ag wire as (pseudo) reference electrode {[nBu₄N][PF₆]} (0.5 M) as electrolyte. Potentials were calibrated against the Fc/Fc⁺ couple (internal standard). NMR spectra were recorded on Bruker AV 300, AV 400 and Avance Neo 400 spectrometers in dry degassed deuterated solvents. ¹H, ¹³C{¹H} chemical shifts were reported against TMS and ³¹P{¹H} against H₃PO₄, CFC₃ for ¹⁹F, NH₃ for ¹⁵N and Y(NO₃)₃ for ⁸⁹Y. Coupling constants (*J*) are given in Hertz as positive values, regardless of their real individual signs. The multiplicity of the signals is indicated as s, d or m for singlet, doublet or multiplet respectively. The assignments were confirmed, as necessary, with the use of 2D NMR correlation experiments. Subscript indexes such as py or im are given for entities belonging to the pyridyl, imine, or hydrazonyl subunits of the ligand, respectively. PGSE NMR diffusion measurements were carried out in a Bruker AV III 500 spectrometer using the stimulated echo pulse sequence.^[33] A rectangular shape was used for the gradient pulses and their strength varied automatically in the course of the experiments. The *D* values were determined from the slope of the regression line ln(*I*/*I*₀) versus *G*², according to Equation (1). *I*/*I*₀ = observed spin echo intensity/intensity without gradients, *G* = gradient strength, Δ = delay between the midpoints of the gradients, *D* = diffusion coefficient, δ = gradient length.

$$\ln\left(\frac{I}{I_0}\right) = -(\gamma\delta)^2 G^2 \left(\Delta - \frac{\delta}{3}\right) D \quad (1)$$

The measurements were carried out without spinning. Gradient calibration was carried out by means of a diffusion measurement of HDO in D₂O (*D*(HDO) = 1.902 × 10⁻⁹ m² s⁻¹).^[47] The experimental error in *D* values was estimated to be smaller than ±2% (3 standard deviations). All of the data leading to the reported *D* values afforded lines whose correlation coefficients were above 0.999. The gradient strength was incremented in 4–8% steps from 2–10% to 98% so that, depending on signal:noise, 12–25 points could be used for regression analysis.

Materials and reagents: The ligands im, py, and the complexes Y(py), La(py), Sm(py), and Lu(py) were prepared according to literature methods.^{[48][49][25]} Note that for the complexes described in this paper, no elemental analyses could be obtained due to the high fluorine content of the samples ([OTf] counter ion).

General method for the synthesis of the κ⁶N donor ligands (S)P[N(Me)N=C(H)-Het]₃ (L with Het = heterocycle) (Table 8): 1,1',1''-Trimethylthiophosphoryltrihydrazid (1.98 g, 10 mmol) and MgSO₄ (0.5 g) were suspended in methanol (20 mL). *N*-heterocycle-carbaldehyd (3.21 g, 30 mmol) in methanol (20 mL) was added dropwise. After addition, the mixture was refluxed overnight. The resulting mixture was cooled down to room temperature and filtered. The

Table 8. Reaction solvent, recrystallization solvent and yield of the ligands.

Ligand	Reaction solvent	Recrystallization solvent	Yield [%]
⁴ Me ₂ im	MeOH/DCM	CHCl ₃ /EtOH	quant.
⁵ Me ₂ pz	MeOH	MeOH/CH ₃ CN	68
pyz	MeOH	CHCl ₃ / <i>n</i> -hexane	89
pydz	MeOH	MeCN	81

solid was extracted with chloroform (3 x 5 mL) and the filtrate was evaporated under reduced pressure. The obtained solid was dissolved in chloroform (20 mL) and overlaid with *n*-hexane (40 mL). The product was obtained as colorless crystals after several recrystallization from acetonitrile.

⁴Me₂im: M.p.: > 155 °C decomp. ¹H NMR (300.13 MHz, 298.8 K, d₆-DMSO): δ = 2.21 (s, 9H, im-Me), 3.16 (d, ²J_{HP} = 9.1 Hz, 9H, N-CH₃), 7.55 (s, 3H), 7.65 (d, ⁴J_{HP} = 1.5 Hz, 3H, N=CH) ppm. ¹³C{¹H} NMR (75.48 MHz, 298.8 K, d₆-DMSO): δ = 11.6 (s, im-Me), 32.8 (d, ²J_{CP} = 8.36 Hz, N-CH₃), 129.1 (s), 130.0 (s), 133.3 (d, ³J_{CP} = 14.9 Hz, N=CH), 135.0 (s) ppm. ³¹P{¹H} NMR (121.49 MHz, 298.8 K, d₆-DMSO): δ = 72.3 (s) ppm. FTIR (solid, ATR): 2223 (w), 2193 (vw), 2082 (vw), 2028 (vw), 1992 (w), 1976 (w), 1959 (w), 1950 (vw), 1931 (vw), 1440 (w), 1386 (w), 1227 (w), 1148 (w), 944 (vs), 867 (s), 753 (s), 703 (m), 641 (s), 632 (s), 613 (vs), 573 (s), 545 (s), 520 (s), 509 (vs), 486 (vs), 467 (vs), 455 (vs), 444 (vs), 433 (vs), 423 (vs), 398 (s), 390 (vs), 381 (s) cm⁻¹.

⁵Me₂pz: M.p.: 130–155 °C. ¹H NMR (300.13 MHz, 298.8 K, CD₃CN): δ = 2.18 (s, 9H, pz-Me), 3.20 (d, ²J_{HP} = 9.1 Hz, 9H, N-CH₃), 6.13 (s, 3H), 7.66 (s, 3H, N=CH), 10.76 (s, br, 3H, N-H) ppm. ¹³C{¹H} NMR (75.48 MHz, 298.8 K, CD₃CN): δ = 11.2 (s, pz-Me), 32.8 (d, ²J_{CP} = 7.90 Hz, N-CH₃), 102.4 (s), 133.5 (s, N=CH) ppm. ³¹P{¹H} NMR (121.49 MHz, 298.8 K, CD₃CN): δ = 72.9 (s) ppm. FTIR (solid, ATR): 2860 (vw), 2157 (w), 2024 (vw), 1572 (vw), 1426 (w), 1225 (w), 1138 (m), 1005 (w), 948 (vs), 846 (s), 799 (m), 758 (vs), 738 (vs), 670 (s), 599 (s), 518 (vs), 471 (vs), 453 (vs), 422 (vs), 407 (vs), 394 (vs) cm⁻¹.

pyz: M.p.: > 210 °C decomp. ¹H NMR (300.13 MHz, 298.8 K, CD₃CN): δ = 3.40 (dd, ³J_{HP} = 9.1 Hz, ⁵J_{HH} = 0.6 Hz, 9H, N-CH₃), 7.23 (ddd, ³J_{HH} = 8.6 Hz, ³J_{HH} = 4.9 Hz, ⁵J_{HH} = 0.7 Hz, 3H), 7.71 (dd, ³J_{HH} = 8.7 Hz, ⁴J_{HH} = 1.7 Hz, 3H), 8.05 (m, ⁴J_{HH} = 0.9 Hz, ⁴J_{HP} = 1.0 Hz, 3H, N=CH), 8.96 (dd, ³J_{HH} = 4.8 Hz, ⁴J_{HH} = 1.8 Hz, 3H) ppm. ¹³C{¹H} NMR (75.48 MHz, 298.8 K, CD₃CN): δ = 33.5 (d, ²J_{CP} = 9.3 Hz, N-CH₃), 123.5 (s), 127.7 (s), 137.4 (d, ³J_{CP} = 14.4 Hz, N=CH), 152.0 (s), 158.6 (s) ppm. ³¹P{¹H} NMR (121.49 MHz, 298.8 K, CD₃CN): δ = 72.8 (s) ppm. FTIR (solid, ATR): 3053 (w), 1590 (m), 1568 (m), 1518 (w), 1458 (m), 1406 (m), 1358 (m), 1222 (m), 1163 (s), 1107 (m), 1057 (w), 1014 (w), 985 (m), 966 (vs), 899 (m), 883 (s), 839 (m), 782 (vs), 752 (m), 706 (m), 666 (m), 630 (s), 611 (m), 582 (m), 530 (m), 515 (s), 463 (s), 413 (vs) cm⁻¹.

pydz: M.p.: > 170 °C decomp. ¹H NMR (300.13 MHz, 298.8 K, CDCl₃): δ = 3.41 (dd, ³J_{HP} = 9.1 Hz, 9H, N-CH₃), 7.80 (d, ³J_{HH} = 1.1 Hz, 3H, N=CH), 8.42 (d, ³J_{HH} = 2.3 Hz, 3H), 8.51 (s, 3H), 8.90 (s, 3H) ppm. ¹³C{¹H} NMR (75.48 MHz, 298.8 K, CDCl₃): δ = 32.9 (d, ²J_{CP} = 9.9 Hz, N-CH₃), 136.0 (d, ³J_{CP} = 14.4 Hz, N=CH), 141.5 (s), 143.0 (s), 143.5 (s), 149.7 (s) ppm. ³¹P{¹H} NMR (121.49 MHz, 298.8 K, CDCl₃): δ = 72.3 (s) ppm. FTIR (solid, ATR): 1590 (w), 1568 (w), 1518 (w), 1458 (w), 1406 (w), 1358 (w), 1222 (m), 1163 (m), 1107 (m), 1057 (w), 1014 (w), 985 (m), 1966 (m), 899 (w), 883 (m), 839 (m), 781 (s), 752 (m), 706 (w), 666 (w), 630 (m), 611 (s), 611 (m), 582 (m), 529 (m), 515 (m), 463 (s), 413 (s) cm⁻¹.

General method for the synthesis of the complexes [(κ⁶N-L)Ln(OTf)₃] (Table 9): Ligand (L) and Ln(OTf)₃ were dissolved in THF in stoichiometric quantities and stirred overnight at room temperature. The precipitate forming was filtered and wash two times with THF. The resulting solid was dissolved in acetonitrile and overlaid

Table 9. Scale, recrystallization solvent and yield of the complexes.

Compound	Scale (μmol)	Recrystallization solvent	Yield [%]
Y(im)	231.2	MeCN/Et ₂ O	85
La(im)	100.0	MeCN/Et ₂ O	82
Sm(im)	231.2	MeCN/Et ₂ O	82
Lu(im)	100.0	MeCN/Et ₂ O	86
Ce(im)	500.0	MeCN/Et ₂ O	92
Ce(⁴ Me ₂ im)	500.0	MeCN/Et ₂ O	92
Y(⁴ Me ₂ im)	250.0	MeCN/Et ₂ O	45
Ce(⁴ Me ₂ im)	500.0	MeCN/Et ₂ O	75
Y(⁵ Me ₂ pz)	250.0	MeCN/ ⁱ Pr ₂ O	75
La(⁵ Me ₂ pz)	105.0	MeCN/Et ₂ O	88
Sm(⁵ Me ₂ pz)	500.0	MeCN/Et ₂ O	97
Lu(⁵ Me ₂ pz)	250.0	MeCN/Et ₂ O	72
Ce(⁵ Me ₂ pz)	127.6	MeCN/ ⁱ Pr ₂ O	58
Ce(py)	500.0	MeCN/Et ₂ O	73

with ether to obtain pure product. (For those where no precipitate forms: the clear solution was evaporated to dryness and the solid dissolved in acetonitrile and overlaid with ether to obtain pure product).

Y(im): M.p.: 271–281 °C. ¹H NMR (300.13 MHz, 298.8 K, CD₃CN): δ = 3.36 (d, ³J_{HP} = 10.8 Hz, 9H, N-CH₃), 7.53 (s, 3H), 8.20 (s, 3H), 8.25 (s, 3H, N=CH), 11.13 (s, br, *W*_{1/2} ≈ 15 Hz, 3H, NH) ppm. ¹³C{¹H} NMR (75.48 MHz, 298.8 K, CD₃CN): δ = 38.1 (d, ²J_{CP} = 7.7 Hz, N-CH₃), 122.7 (s), 134.8 (s), 140.8 (s), 148.9 (d, ³J_{CP} = 9.9 Hz, N=CH) ppm. ¹⁹F{¹H} NMR (282.40 MHz, 298.8 K, CD₃CN): δ = -79.4 (s) ppm. ³¹P{¹H} NMR (121.49 MHz, 298.8 K, CD₃CN): δ = 65.8 (s) ppm. ⁸⁹Y NMR (19.61 MHz, 298.8 K, CD₃CN): δ = 24.8 (s) ppm. FTIR (solid, ATR): 3201 (vw), 3132 (w), 2947 (vw), 2898 (vw), 2262 (w), 1612 (vw), 1537 (vw), 1514 (vw), 1444 (w), 1419 (vw), 1316 (m), 1303 (m), 1258 (vs), 1241 (vs), 1211 (vs), 1166 (vs), 1059 (s), 1038 (s), 1027 (vs), 994 (w), 957 (s), 862 (m), 850 (m), 795 (s), 767 (s), 715 (m), 633 (vs), 619 (vs), 585 (m), 515 (m), 497 (s), 481 (m) cm⁻¹.

La(im): M.p.: > 190 °C decomp. ¹H NMR (300.13 MHz, 298.8 K, CD₃CN): δ = 3.37 (d, ³J_{HP} = 10.2 Hz, 9H, N-CH₃), 7.52 (d, ⁴J_{HH} = 0.9 Hz, 3H), 8.09 (s, 3H), 8.24 (s, 3H, N=CH), 10.85 (s, br, *W*_{1/2} ≈ 23 Hz, 3H, NH) ppm. ¹³C{¹H} NMR (75.48 MHz, 298.8 K, CD₃CN): δ = 38.0 (d, ²J_{CP} = 8.0 Hz, N-CH₃), 123.1 (s), 135.4 (s), 140.0 (s), 149.0 (s, N=CH) ppm. ¹⁹F{¹H} NMR (282.40 MHz, 298.8 K, CD₃CN): δ = -79.4 (s) ppm. ³¹P{¹H} NMR (121.49 MHz, 298.8 K, CD₃CN): δ = 67.4 (s) ppm. FTIR (solid, ATR): 1615 (vw), 1511 (vw), 1445 (vw), 1296 (w), 1216 (m), 1170 (w), 1089 (w), 1027 (s), 953 (m), 853 (w), 758 (m), 719 (w), 631 (vs), 614 (s), 583 (w), 511 (s), 481 (m) cm⁻¹.

Sm(im): M.p.: 256–258 °C. ¹H NMR (300.13 MHz, 298.8 K, CD₃CN): δ = 2.76 (d, ³J_{HP} = 10.6 Hz, 9H, N-CH₃), 8.11 (s, 3H), 8.23 (d, ⁴J_{HH} = 1.5 Hz, 3H), 8.26 (s, 3H, N=CH), 11.42 (s, br, *W*_{1/2} ≈ 17 Hz, 3H, NH) ppm. ¹³C{¹H} NMR (75.48 MHz, 298.8 K, CD₃CN): δ = 31.4 (d, ²J_{CP} = 7.63 Hz, N-CH₃), 123.7 (s), 140.3 (s), 141.6 (s), 151.9 (s, N=CH) ppm. ¹⁹F{¹H} NMR (282.40 MHz, 298.8 K, CD₃CN): δ = -79.5 (s) ppm. ³¹P{¹H} NMR (121.49 MHz, 298.8 K, CD₃CN): δ = 64.0 (s) ppm. FTIR (solid, ATR): 3524 (br), 3132 (vw), 3057 (vw), 2599 (vw), 1616 (w), 1515 (w), 1447 (w), 1286 (m), 1254 (m), 1218 (vs), 1168 (m), 1093 (m), 1034 (vs), 956 (s), 917 (w), 854 (s), 763 (s), 721 (w), 697 (vw), 632 (vs), 612 (s), 583 (m), 573 (m), 512 (s), 484 (m), 415 (vw) cm⁻¹.

Lu(im): M.p.: 190–200 °C. ¹H NMR (300.13 MHz, 298.8 K, CD₃CN): δ = 3.39 (d, ³J_{HP} = 11.0 Hz, 9H, N-CH₃), 7.58 (s, 3H), 8.24 (s,

3H), 8.28 (s, 3H, N=CH), 11.44 (s, br, $W_{1/2} \approx 17.4$ Hz, 3H, NH) ppm. $^{13}\text{C}\{^1\text{H}\}$ NMR (75.48 MHz, 298.8 K, CD_3CN): $\delta = 37.7$ (d, $^2J_{\text{CP}} = 8.0$ Hz, N-CH₃), 122.7 (s), 135.1 (s), 142.4 (s) and 147.7 (d, $^3J_{\text{CP}} = 9.9$ Hz, N=CH) ppm. $^{19}\text{F}\{^1\text{H}\}$ NMR (282.40 MHz, 298.8 K, CD_3CN): $\delta = -79.4$ (s) ppm. $^{31}\text{P}\{^1\text{H}\}$ NMR (121.49 MHz, 298.8 K, CD_3CN): $\delta = 65.5$ (s) ppm. FTIR (Feststoff, ATR): 3194 (br), 3135 (br), 3052 (w), 2947 (vw), 2901 (vw), 2261 (vw), 2153 (vw), 1614 (w), 1538 (vw), 1515 (vw), 1444 (w), 1419 (m), 1361 (s), 1303 (s), 1242 (vs), 1213 (vs), 1164 (s), 1089 (m), 1039 (m), 1026 (s), 995 (m), 959 (s), 863 (m), 796 (s), 768 (s), 727 (m), 716 (m), 632 (vs), 618 (s), 574 (m), 516 (s), 482 (s) cm^{-1} .

Ce(im): M.p.: > 250 °C decomp. ^1H NMR (300.13 MHz, 298.8 K, CD_3CN): $\delta = 0.71$ (s, br, 9H, N-CH₃), 8.51 (s, br, 3H), 10.81 (s, br, 3H), 12.03 (s, br, 3H), 13.75 (s, br, 3H) ppm. $^{13}\text{C}\{^1\text{H}\}$ NMR (75.48 MHz, 298.8 K, CD_3CN): $\delta = 34.7$ (s, N-CH₃), 46.1 (s), 121.0 (s), 124.3 (s), 131.0 (s), 140.4 (s), 149.9 (s), 151.6 (s) ppm. $^{19}\text{F}\{^1\text{H}\}$ NMR (282.40 MHz, 298.8 K, CD_3CN): $\delta = -79.8$ (s) ppm. $^{31}\text{P}\{^1\text{H}\}$ NMR (121.49 MHz, 298.8 K, CD_3CN): $\delta = 58.2$ (s) ppm. FTIR (solid, ATR): 3185 (vw), 1613 (vw), 1512 (vw), 1447 (vw), 1297 (w), 1216 (s), 1167 (m), 1089 (w), 1027 (s), 956 (m), 858 (m), 761 (m), 719 (w), 633 (vs), 615 (s), 573 (w), 513 (s), 482 (m), 443 (w), 415 (w), 394 (w), 386 (w) cm^{-1} .

Ce(Me₂im): M.p.: > 160 °C decomp. ^1H NMR (300.13 MHz, 298.8 K, CD_3CN): $\delta = 0.12$ (d, $^3J_{\text{HP}} = 10.2$ Hz, 9H, N-CH₃), 6.13 (s, 9H, N_{im}-Me), 7.58 (s, 3H), 10.21 (s, 3H), 11.74 (s, br, 3H, N=CH) ppm. $^{13}\text{C}\{^1\text{H}\}$ NMR (75.48 MHz, 298.8 K, CD_3CN): $\delta = 33.2$ (d, $^2J_{\text{CP}} = 9.81$ Hz, N-CH₃), 37.4 (s, N_{im}-Me), 135.1 (s), 138.5 (s), 141.3 (d, $^3J_{\text{CP}} = 11.26$ Hz, N=CH), 152.3 (s) ppm. $^{19}\text{F}\{^1\text{H}\}$ NMR (282.40 MHz, 298.8 K, CD_3CN): $\delta = -74.8$ (s) ppm. $^{31}\text{P}\{^1\text{H}\}$ NMR (121.49 MHz, 298.8 K, CD_3CN): $\delta = 53.0$ (s) ppm. FTIR (solid, ATR): 2165 (vw), 2140 (vw), 2026 (vw), 1967 (vw), 1489 (vw), 1451 (vw), 1424 (vw), 1307 (w), 1233 (s), 1211 (vs), 1169 (m), 1027 (s), 963 (s), 886 (w), 775 (w), 713 (vw), 683 (vw), 634 (vs), 572 (vw), 533 (vw), 511 (m), 491 (w), 411 (vw), 391 (w) cm^{-1} .

Y(4Me₂im): M.p.: > 200 °C decomp. ^1H NMR (400 MHz, 298.8 K, CD_3CN): $\delta = 2.37$ (s, 9H, im-CH₃), 3.35 (d, $^3J_{\text{HP}} = 10.9$ Hz, 9H, N-CH₃), 8.06 (s, 3H, im-H), 8.21 (s, 3H, N=CH), 11.10 (s, 3H, NH) ppm. $^{13}\text{C}\{^1\text{H}\}$ NMR (100.6 MHz, 298.8 K, CD_3CN): $\delta = 9.6$ (s, im-CH₃), 38.1 (s, N-CH₃), 131.0 (s), 134.3 (s), 140.0 (s), 149.4 (s, N=CH) ppm. ^{19}F NMR (282.40 MHz, 298.8 K, CD_3CN): $\delta = -79.3$ (s) ppm. $^{31}\text{P}\{^1\text{H}\}$ NMR (121.4 MHz, 298.8 K, CD_3CN): $\delta = 66.7$ (s) ppm. ^{89}Y NMR (19.61 MHz, 298.8 K, CD_3CN): $\delta = 56.6$ (s) ppm. FTIR (solid, ATR): 3197 (vw), 2169 (vw), 1629 (vw), 1447 (vw), 1289 (w), 1213 (m), 1165 (m), 1027 (s), 961 (m), 875 (m), 774 (m), 635 (vs), 573 (m), 513 (s), 381 (m) cm^{-1} .

La(4Me₂im): ^1H NMR (400.1 MHz, 298.8 K, CD_3CN): $\delta = 2.36$ (s, 9H, im-CH₃), 3.35 (d, $^3J_{\text{HP}} = 10.4$ Hz, 9H, N-CH₃), 7.96 (s, 3H, im-H), 8.20 (s, 3H, N=CH), 10.79 (s, 3H, NH) ppm. $^{13}\text{C}\{^1\text{H}\}$ NMR (100.6 MHz, 298.8 K, CD_3CN): $\delta = 9.6$ (s, im-CH₃), 38.0 (d, $^2J_{\text{CP}} = 7.63$ Hz, N-CH₃), 131.4 (s), 134.3 (s), 138.9 (s, C_{im}-H), 149.3 (s, N=CH) ppm. ^{19}F NMR (282.40 MHz, 298.8 K, 298.8 K, CD_3CN): $\delta = -79.4$ (s) ppm. $^{31}\text{P}\{^1\text{H}\}$ NMR (121.4 MHz, 298.8 K, CD_3CN): $\delta = 68.5$ (s) ppm.

Sm(4Me₂im): ^1H NMR (400.1 MHz, 298.8 K, CD_3CN): $\delta = 2.76$ (d, $^3J_{\text{HP}} = 7.1$ Hz, 9H, N-CH₃), 2.82 (s, 9H, im-CH₃), 8.07 (s, 3H, im-H), 8.22 (s, 3H, N=CH), 11.19 (s, 3H, NH) ppm. $^{13}\text{C}\{^1\text{H}\}$ NMR (100.6 MHz, 298.8 K, CD_3CN): $\delta = 10.2$ (s, im-CH₃), 37.2 (s, N-CH₃), 135.1 (s), 136.5 (s), 140.6 (s, C_{im}-H), 152.5 (s, N=CH) ppm. ^{19}F NMR (282.40 MHz, 298.8 K, 298.8 K, CD_3CN): $\delta = -79.5$ (s) ppm. $^{31}\text{P}\{^1\text{H}\}$ NMR (121.4 MHz, 298.8 K, CD_3CN): $\delta = 65.2$ (s) ppm.

Lu(4Me₂im): ^1H NMR (400.1 MHz, 298.8 K, CD_3CN): $\delta = 2.38$ (s, 9H, im-CH₃), 3.38 (d, $^3J_{\text{HP}} = 11.0$ Hz, 9H, N-CH₃), 8.10 (s, 3H, im-H), 8.24 (s, 3H, N=CH), 11.05 (s, 3H, NH) ppm. $^{13}\text{C}\{^1\text{H}\}$ NMR (100.6 MHz, 298.8 K, CD_3CN): $\delta = 9.6$ (s, im-CH₃), 37.9 (d, $^2J_{\text{CP}} = 7.27$ Hz, N-CH₃), 123.23 (s), 131.3 (s), 134.4 (s), 141.4 (s, C_{im}-H), 148.7 (s, N=CH) ppm. ^{19}F NMR (282.40 MHz, 298.8 K, 298.8 K, CD_3CN): $\delta = -79.5$ (s) ppm. $^{31}\text{P}\{^1\text{H}\}$ NMR (121.4 MHz, 298.8 K, CD_3CN): $\delta = 66.8$ (s) ppm.

Ce(4Me₂im): M.p.: > 240 °C decomp. ^1H NMR (400.1 MHz, 298.8 K, CD_3CN): $\delta = 0.74$ (s, br, 9H, N-CH₃), 4.24 (s, br, 9H, im-CH₃), 9.33 (s, br, 3H), 12.30 (s, br, 3H), 13.93 (s, br, 3H) ppm. $^{13}\text{C}\{^1\text{H}\}$ NMR (100.6 MHz, 298.8 K, CD_3CN): $\delta = 12.38$ (im-CH₃), 34.83 (N-CH₃), 137.47, 142.81, 151.33 (im-CH) ppm. ^{19}F NMR (282.40 MHz, 298.8 K, CD_3CN): $\delta = -79.77$ (s) ppm. $^{31}\text{P}\{^1\text{H}\}$ NMR (121.4 MHz, 298.8 K, CD_3CN): $\delta = 59.75$ (s) ppm. FTIR (solid, ATR): 2183 (vw), 2145 (vw), 1993 (vw), 1622 (vw), 1445 (vw), 1305 (vw), 1212 (m), 1167 (w), 1029 (m), 956 (w), 880 (w), 765 (w), 702 (vw), 634 (vs), 580 (vw), 512 (m), 490 (w), 417 (vw), 401 (w), 386 (vw) cm^{-1} .

Y(5Me₂pz): M.p.: > 290 °C decomp. $^1\text{H}\{^{31}\text{P}\}$ NMR (300.13 MHz, 298.8 K, CD_3CN): $\delta = 2.38$ (s, 9H, pz-Me), 3.41 (s, 9H, N-CH₃), 6.47 (s, 3H), 8.18 (s, 3H, N=CH), 11.66 (s, br, 3H, NH) ppm. $^{13}\text{C}\{^1\text{H}\}$ NMR (100.61 MHz, 298.8 K, CD_3CN): $\delta = 10.9$ (s, pz-Me), 37.9 (d, $^2J_{\text{CP}} = 9.2$ Hz, N-CH₃), 108.1 (s), 144.7 (s), 146.6 (d, $^3J_{\text{CP}} = 14.4$ Hz, N=CH), 146.9 (s) ppm. $^{19}\text{F}\{^1\text{H}\}$ NMR (282.40 MHz, 298.8 K, CD_3CN): $\delta = -79.3$ (s) ppm. $^{31}\text{P}\{^1\text{H}\}$ NMR (121.49 MHz, 298.8 K, CD_3CN): $\delta = 64.4$ (s) ppm. ^{89}Y NMR (19.61 MHz, CD_3CN): $\delta = -17.8$ (s) ppm. FTIR (solid, ATR): 3476 (w), 3286 (br), 3153 (w), 298.80 (w), 1572 (m), 1480 (w), 1435 (m), 1307 (s), 1236 (vs), 1216 (vs), 1164 (s), 1063 (w), 1033 (vs), 994 (vs), 957 (m), 912 (m), 879 (m), 867 (m), 813 (w), 778 (w), 751 (w), 740 (w), 691 (w), 633 (vs), 584 (w), 572 (w), 555 (m), 529 (s), 516 (s), 479 (m) cm^{-1} .

La(5Me₂pz): M.p.: 234–259 °C. ^1H NMR (300.13 MHz, 298.8 K, CD_3CN): $\delta = 2.35$ (s, 9H, pz-Me), 3.41 (d, $^3J_{\text{HP}} = 10.6$ Hz, 9H, N-CH₃), 6.45 (dd, $^4J_{\text{HH}} = 1.3$ Hz, $^5J_{\text{HH}} = 0.6$ Hz, 3H), 8.13 (d, $^4J_{\text{HP}} = 0.9$ Hz, 3H, N=CH), 11.45 (s, br, 3H, NH) ppm. $^{13}\text{C}\{^1\text{H}\}$ NMR (75.48 MHz, 298.8 K, CD_3CN): $\delta = 11.2$ (s, pz-Me), 37.3 (d, $^2J_{\text{CP}} = 9.3$ Hz, N-CH₃), 108.3 (s), 144.4 (s), 145.6 (d, $^3J_{\text{CP}} = 13.1$ Hz, N=CH), 148.1 (s, 3-C_{pz}) ppm. $^{19}\text{F}\{^1\text{H}\}$ NMR (282.40 MHz, 298.8 K, CD_3CN): $\delta = -79.2$ (s) ppm. $^{31}\text{P}\{^1\text{H}\}$ NMR (121.49 MHz, 298.8 K, CD_3CN): $\delta = 68.5$ (s) ppm. FTIR (solid, ATR): 1994 (vw), 1956 (vw), 1573 (vw), 1428 (vw), 1311 (w), 1233 (m), 1216 (m), 1165 (m), 1024 (s), 957 (m), 872 (w), 774 (w), 689 (vw), 633 (vs), 570 (vw), 513 (s), 476 (w), 414 (w) cm^{-1} .

Sm(5Me₂pz): M.p.: > 295 °C decomp. ^1H NMR (300.13 MHz, 298.8 K, CD_3CN): $\delta = 2.55$ (s, 9H, pz-Me), 2.74 (d, $^4J_{\text{HH}} = 10.3$ Hz, 9H, N-CH₃), 7.12 (s, 3H), 8.16 (s, 3H, N=CH), 11.12 (s, br, 3H, N-H) ppm. $^{13}\text{C}\{^1\text{H}\}$ NMR (75.48 MHz, 298.8 K, CD_3CN): $\delta = 11.1$ (s, pz-Me), 36.5 (d, $^2J_{\text{CP}} = 8.98$ Hz, N-CH₃), 109.1 (s), 145.0 (s, N=CH), 148.7 (s), 152.1 (s) ppm. ^{19}F NMR (282.40 MHz, 298.8 K, CD_3CN): $\delta = -79.3$ (s) ppm. $^{31}\text{P}\{^1\text{H}\}$ NMR (121.49 MHz, 298.8 K, CD_3CN): $\delta = 62.1$ (s) ppm. FTIR (solid, ATR): 1575 (vw), 1430 (vw), 1307 (w), 1216 (m), 1173 (w), 1143 (w), 1027 (m), 986 (vw), 951 (w), 913 (vw), 873 (w), 817 (vw), 774 (w), 695 (vw), 656 (vw), 634 (vs), 583 (vw), 571 (vw), 517 (s), 477 (m), 401 (vw), 386 (vw) cm^{-1} .

Lu(5Me₂pz): M.p.: 124–126 °C. ^1H NMR (300.13 MHz, 298.8 K, CD_3CN): $\delta = 2.45$ (d, $^4J_{\text{HH}} = 0.4$ Hz, 9H, pz-Me), 3.46 (dd, $^3J_{\text{HP}} = 10.7$ Hz, $^5J_{\text{HH}} = 0.6$ Hz, 9H, N-CH₃), 6.55 (s, 3H, 4-H_{pz}), 8.19 („dq“, $^4J_{\text{HP}} = 1.5$ Hz, $^5J_{\text{HH}} = 0.8$ Hz, 3H, N=CH), 12.13 (s, br, 3H, NH) ppm. $^{13}\text{C}\{^1\text{H}\}$ NMR (75.48 MHz, 298.8 K, CD_3CN): $\delta = 11.0$ (s, pz-Me), 37.6 (d, $^2J_{\text{CP}} = 9.3$ Hz, N-CH₃), 108.6 (s, 4-C_{pz}), 144.0 (d, $^3J_{\text{CP}} = 14.4$ Hz, N=CH), 147.7 (s, 5-C_{pz}), 148.5 (s, 3-C_{pz}) ppm. $^{19}\text{F}\{^1\text{H}\}$ NMR (282.40 MHz, 298.8 K, CD_3CN): $\delta = -79.3$ (s) ppm. $^{31}\text{P}\{^1\text{H}\}$ NMR (121.49 MHz, 298.8 K, CD_3CN): $\delta = 63.3$ (s) ppm. FTIR (solid, ATR): 3475 (w), 3276 (br), 3155 (w), 298.82 (w), 1573 (m), 1481 (w), 1437 (m), 1308 (s), 1251 (vs), 1236 (vs), 1216 (vs), 11164 (s), 1063 (vs), 1031 (vs), 996 (m), 956 (s), 912 (w), 880 (m), 867 (m), 814 (m), 780 (m), 753 (s), 741 (w), 691 (w), 649 (w), 632 (vs), 584 (m), 572 (m), 555 (m), 530 (m), 517 (s), 480 (m) cm^{-1} .

Ce(5Me₂pz): M.p.: > 304 °C decomposed. ^1H NMR (300.13 MHz, 298.8 K, CD_3CN): $\delta = 0.70$ (s, br, 9H, N-CH₃), 2.83 (s, 9H, N=CH), 9.11 (s, br, 3H), 11.06 (s, br, 3H) ppm. $^{13}\text{C}\{^1\text{H}\}$ NMR (75.48 MHz, CD_3CN): $\delta = 12.0$ (s, pz-Me), 33.7 (d, $^2J_{\text{CP}} = 8.72$ Hz, N-CH₃), 114.8 (s), 142.8 (s),

151.3 (s), 152.2 (s) ppm. ^{19}F NMR (282.40 MHz, 298.8 K, CD_3CN): $\delta = 79.0$ (s) ppm. ^{31}P NMR (121.49 MHz, 298.8 K, CD_3CN): $\delta = 54.8$ (s) ppm. FTIR (solid, ATR): 1571 (vw), 1475 (vw), 1430 (vw), 1304 (s), 1235 (s), 1213 (vs), 1163 (s), 1027 (vs), 959 (s), 912 (vw), 877 (w), 866 (w), 811 (vw), 773 (m), 737 (vw), 690 (vw), 634 (vs), 571 (vw), 555 (vw), 515 (s), 475 (w) cm^{-1} .

Ce(py): M.p.: $> 300^\circ\text{C}$ decomposed. ^1H NMR (400.1 MHz, 298.8 K, CD_3CN): $\delta = 0.75$ (s, br, 9H, N-CH_3), 7.58 (s, br, 3H), 9.39 (t, br, $J_{\text{HH}} = 7.9$ Hz, 3H), 10.28 (s, br, 3H), 11.47 (s, br, 3H) ppm. $^{13}\text{C}\{^1\text{H}\}$ NMR (100.6 MHz, 298.8 K, CD_3CN): $\delta = 33.3$ (N-CH_3), 129.5 (s), 134.1 (s), 142.4 (s), 147.1 (s), 151.9 (s), 156.1 (N=CH) ppm. ^{19}F NMR (282.40 MHz, 298.8 K, CD_3CN): $\delta = -78.3$ ppm. ^{31}P NMR (121.4 MHz, 298.8 K, CD_3CN): $\delta = 55.7$ ppm. FTIR (solid, ATR): 1608 (vw), 1563 (vw), 1441 (vw), 1305 (w), 1234 (w), 1198 (m), 1181 (w), 1150 (m), 1105 (vw), 1026 (m), 1008 (m), 955 (m), 790 (m), 777 (m), 765 (m), 701 (vw), 630 (vs), 601 (w), 581 (vw), 570 (vw), 510 (s), 466 (w), 414 (w) cm^{-1} .

Crystallographic details: Deposition Number(s) 2245061 (for Lu(im)), 2244878 (for Ce(im)), 2244876 (for Ce($^{4\text{Me}}$ im)), 2244880 (for Y($^{5\text{Me}}$ pz)), 2244883 (for La($^{5\text{Me}}$ pz)), 2244877 (for Ce($^{5\text{Me}}$ pz)), 2244882 (for pyz), and 2245330 (for Ce(py)) contain(s) the supplementary crystallographic data for this paper.

Supporting Information

Additional references cited within the Supporting Information.^[50–66] The Supporting Information also contain cyclic voltammograms, crystallographic Data, NMR Spectra, details re the competition Studies, VT ^{19}F NMR spectra, further computational details, and the coordinates of the calculated structures.

Acknowledgements

Support by the Federal Ministry of Education and Research (BMBF Project No. 02NUK059F) is also gratefully acknowledged. The authors further acknowledge support by the state of Baden-Württemberg through bwHPC, the German Research Foundation (DFG) through grant no INST 40/575-1 FUGG (JUSTUS 2 cluster), Junta de Andalucía (102C2000004, UAL2020-AGR-B1781 and P20_01041) and the State Research Agency of the Spanish Ministry of Science, Innovation and Universities (PID2021-126445OB-I00, PDC2021-121248-I00 and PLEC2021-007774), together with EU FEDER funds. Open Access funding enabled and organized by Projekt DEAL.

Conflict of Interests

The authors declare no conflict of interest.

Data Availability Statement

The data that support the findings of this study are available in the supplementary material of this article.

Keywords: extraction ligands · lanthanides · nitrogen ligands · NMR spectroscopy · quantum chemistry

- [1] a) H. Schumann, J. A. Meese-Marktscheffel, L. Esser, *Chem. Rev.* **1995**, *95*, 865; b) J. P. Collman, *Principles and applications of organotransition metal chemistry*, Univ. Science Books, Mill Valley, Calif., **1987**; c) A. J. Freeman, R. E. Watson, *Phys. Rev.* **1962**, *127*, 2058; d) N. Kaltsoyannis, P. Scott, *The f elements*, Oxford University Press, Oxford, **1999**; e) P. W. Roesky, *Molecular Catalysis of Rare-Earth Elements*, Springer Berlin/Heidelberg, Berlin, Heidelberg, **2010**.
- [2] R. G. Pearson, *J. Am. Chem. Soc.* **1963**, *85*, 3533.
- [3] S. Cotton, *Lanthanide and Actinide Chemistry*, John Wiley & Sons Ltd, Hoboken, **2007**.
- [4] a) P. W. Roesky, M. T. Gamer, N. Marinos, *Chem. Eur. J.* **2004**, *10*, 3537; b) P. W. Roesky, M. T. Gamer, M. Puchner, A. Greiner, *Chem. Eur. J.* **2002**, *8*, 5265; c) J. Scholz, H. Görls, H. Schumann, R. Weimann, *Organometallics* **2001**, *20*, 4394; d) T. G. Wetzel, S. Dehnen, P. W. Roesky, *Angew. Chem. Int. Ed.* **1999**, *38*, 1086; e) H. Yan, J. Wei, W.-X. Zhang, *Organometallics* **2021**, *40*, 3245.
- [5] F. T. Edelmann, *Chem. Soc. Rev.* **2009**, *38*, 2253.
- [6] a) F. Kong, M. Li, X. Zhou, L. Zhang, *RSC Adv.* **2017**, *7*, 29752; b) Z. Lu, G. P. A. Yap, D. S. Richeson, *Organometallics* **2001**, *20*, 706.
- [7] a) M. Khorasani-Motlagh, M. Noroozifar, S. Niromand, S. Khajeh, B. O. Patrick, *Inorg. Chim. Acta* **2009**, *362*, 3785; b) M. M. Maiwald, A. T. Wagner, J. Kratsch, A. Skerencak-Frech, M. Trumm, A. Geist, P. W. Roesky, P. J. Panak, *Dalton Trans.* **2017**, *46*, 9981; c) C. Kachi-Terajima, K. Yanagi, T. Kaziki, T. Kitazawa, M. Hasegawa, *Dalton Trans.* **2011**, *40*, 2249; d) D. M. Czakis-Sulikowska, J. Radwanska-Doczekalska, *J. Inorg. Nucl. Chem.* **1979**, *41*, 1299.
- [8] a) R. C. Howell, K. V. N. Spence, I. A. Kahwa, A. J. P. White, D. J. Williams, *J. Chem. Soc. Dalton Trans.* **1996**, 961; b) M. T. Kaczmarek, M. Zabiszak, M. Nowak, R. Jastrzab, *Coord. Chem. Rev.* **2018**, *370*, 42; c) H. C. Aspinall, *Chem. Rev.* **2002**, *102*, 1807.
- [9] a) H. C. Aspinall, N. Greeves, *J. Organomet. Chem.* **2002**, *647*, 151; b) S. Mishra, *Coord. Chem. Rev.* **2008**, *252*, 1996.
- [10] a) C. D. Hubbard, R. van Eldik (Eds.) *Adv. Inorg. Chem.*, v.61, Elsevier textbooks, s.l., **2009**; b) V. Kubiček, É. Tóth in *Adv. Inorg. Chem.*, v.61 (Eds.: C. D. Hubbard, R. van Eldik), Elsevier textbooks, s.l., **2009**, pp. 63–129; c) S. Liu, *Chem. Soc. Rev.* **2004**, *33*, 445; d) M. P. Lowe, *Aust. J. Chem.* **2002**, *55*, 551; e) M. Woods, D. E. Woessner, A. D. Sherry, *Chem. Soc. Rev.* **2006**, *35*, 500.
- [11] a) J.-C. G. Bünzli, C. Piguet, *Chem. Soc. Rev.* **2005**, *34*, 1048; b) S. V. Eliseeva, J.-C. G. Bünzli, *Chem. Soc. Rev.* **2010**, *39*, 189; c) S. Faulkner, L. S. Natrajan, W. S. Perry, D. Sykes, *Dalton Trans.* **2009**, 3890.
- [12] a) M. Andruh, J.-P. Costes, C. Diaz, S. Gao, *Inorg. Chem.* **2009**, *48*, 3342; b) C. Benelli, D. Gatteschi, *Chem. Rev.* **2002**, *102*, 2369.
- [13] a) B. B. Beele, U. Müllich, F. Schwörer, A. Geist, P. J. Panak, *Procedia Chem.* **2012**, *7*, 146; b) T. Mangin, R. Schurhammer, G. Wipff, *J. Phys. Chem. B* **2022**, *126*, 2876.
- [14] a) L. Xu, N. Pu, Y. Li, P. Wei, T. Sun, C. Xiao, J. Chen, C. Xu, *Inorg. Chem.* **2019**, *58*, 4420; b) A. V. Zaytsev, R. Bulmer, V. N. Kozhevnikov, M. Sims, G. Modolo, A. Wilden, P. G. Waddell, A. Geist, P. J. Panak, P. Wessling, F. W. Lewis, *Chem. Eur. J.* **2020**, *26*, 428.
- [15] C. Fazio, J. U. Knebel, W. Tromm, A. Geist, K. Gompfer, *Nachr. Forschungszent. Karlsruhe* **2006**, 37.
- [16] L. H. Baetsle, T. Wakabayashi, S. Sakurai, *Status and assessment report on actinide and fission product partitioning and transmutation*, OECD-NEA, Nuclear Energy Agency of the OECD (NEA), **1999**.
- [17] L. Giusti, *Waste Manage.* **2009**, *29*, 2227.
- [18] R. Busquim e Silva, M. S. Kazimi, P. Hejzlar, *Energy Environ. Sci.* **2010**, *3*, 996.
- [19] IAEA, *Status and Trends in Spent Fuel Reprocessing 1999*.
- [20] a) O. Courson, M. Lebrun, R. Malmbeck, G. Pagliosa, K. Römer, B. Sätmark, J.-P. Glatz, *Radiochim. Acta* **2000**, *88*, 857; b) D. Serrano-Purroy, B. Christiansen, J.-P. Glatz, R. Malmbeck, G. Modolo, *Radiochim. Acta* **2005**, 351; c) D. Serrano-Purroy, P. Baron, B. Christiansen, R. Malmbeck, C. Sorel, J.-P. Glatz, *Radiochim. Acta* **2005**, *93*, 351.
- [21] a) A. Geist, C. Hill, G. Modolo, M. R. J. St. Foreman, M. Weigl, K. Gompfer, M. J. Hudson, *Solvent Extr. Ion Exch.* **2006**, *24*, 463; b) F. W. Lewis, L. M. Harwood, M. J. Hudson, M. G. B. Drew, J. F. Desreux, G. Vidick, N. Bouslimani, G. Modolo, A. Wilden, M. Sypula, T.-H. Vu, J.-P. Simonin, *J. Am. Chem. Soc.* **2011**, *133*, 13093; c) M. R. J. St. Foreman, M. J. Hudson, A. Geist, C. Madic, M. Weigl, *Solvent Extr. Ion Exch.* **2005**, *23*, 645.

- [22] A. S. Gerasimov, T. S. Zaritskaya, G. V. Kiselev, L. A. Myrtsyomova, *Atomic Energy* **2000**, *89*, 663.
- [23] a) H. H. Dam, D. N. Reinhoudt, W. Verboom, *Chem. Soc. Rev.* **2007**, *36*, 367; b) J. N. Mathur, M. S. Murali, K. L. Nash, *Solvent Extr. Ion Exch.* **2001**, *19*, 357.
- [24] a) M. A. Denecke, P. J. Panak, F. Burdet, M. Weigl, A. Geist, R. Klenze, M. Mazzanti, K. Gommer, *C. R. Chim.* **2007**, *10*, 872; b) D. Guillaumont, *J. Phys. Chem. A* **2004**, *108*, 6893; c) M. A. Denecke, A. Rossberg, P. J. Panak, M. Weigl, B. Schimmelpennig, A. Geist, *Inorg. Chem.* **2005**, *44*, 8418; d) Z. Kolarik, *Chem. Rev.* **2008**, *108*, 4208; e) M. Miguiditchian, D. Guillaumont, D. Guillaumont, P. Moisy, C. Madic, M. P. Jensen, K. L. Nash, *Inorg. Chem.* **2005**, *44*, 1404; f) L. Petit, C. Adamo, P. Maldivi, *Inorg. Chem.* **2006**, *45*, 8517; g) L. Petit, C. Daul, C. Adamo, P. Maldivi, *New J. Chem.* **2007**, *31*, 1738.
- [25] M. W. Löble, P. Oña-Burgos, I. Fernández, C. Apostolidis, A. Morgenstern, O. Walter, F. Bruchertseifer, P. Kaden, T. Vitova, J. Rothe, K. Dardenne, N. L. Banik, A. Geist, M. A. Denecke, F. Breher, *Chem. Sci.* **2013**, *4*, 3717.
- [26] P. Stock, E. Deck, S. Hohnstein, J. Korzekwa, K. Meyer, F. W. Heinemann, F. Breher, G. Hörner, *Inorg. Chem.* **2016**, *55*, 5254.
- [27] A. Paulenova, S. E. Creager, J. D. Navratil, Y. Wei, *J. Power Sources* **2002**, *109*, 431.
- [28] a) G. Canard, S. Koeller, G. Bernardinelli, C. Piguet, *J. Am. Chem. Soc.* **2008**, *130*, 1025; b) M. G. Drew, M. R. Foreman, M. J. Hudson, K. F. Kennedy, *Inorg. Chim. Acta* **2004**, *357*, 4102.
- [29] a) S. Alvarez, *Chem. Rev.* **2015**, *115*, 13447; b) S. Alvarez, D. Avnir, M. Llunell, M. Pinsky, *New J. Chem.* **2002**, *26*, 996.
- [30] L. Falivene, Z. Cao, A. Petta, L. Serra, A. Poater, R. Oliva, V. Scarano, L. Cavallo, *Nat. Chem.* **2019**, *11*, 872.
- [31] A. Poater, F. Ragone, R. Mariz, R. Dorta, L. Cavallo, *Chem. Eur. J.* **2010**, *16*, 14348.
- [32] C. S. Johnson, *Prog. Nucl. Magn. Reson. Spectrosc.* **1999**, *34*, 203.
- [33] P. Stilbs, *Prog. Nucl. Magn. Reson. Spectrosc.* **1987**, *19*, 1.
- [34] a) P. S. Pregosin, *Prog. Nucl. Magn. Reson. Spectrosc.* **2006**, *49*, 261; b) P. S. Pregosin, *Pure Appl. Chem.* **2009**, *81*, 615; c) P. S. Pregosin, E. Martínez-Viviente, P. G. A. Kumar, *Dalton Trans.* **2003**, 4007.
- [35] C. L. Yaws, *Chemical properties handbook. Physical, thermodynamic, environmental, transport, and health related properties for organic and inorganic chemicals*, McGraw-Hill Education; McGraw Hill, New York, N. Y., **1999**.
- [36] R. E. White, T. P. Hanusa, *Organometallics* **2006**, *25*, 5621.
- [37] Y. Xing, A. K. Jindal, M. Regueiro-Figueroa, M. Le Fur, N. Kervarec, P. Zhao, Z. Kovacs, L. Valencia, P. Pérez-Lourido, R. Tripiet, D. Esteban-Gómez, C. Platas-Iglesias, A. D. Sherry, *Chem. Eur. J.* **2016**, *22*, 16657.
- [38] A. N. Gaiser, C. Celis-Barros, F. D. White, M. J. Beltran-Leiva, J. M. Sperling, S. R. Salpage, T. N. Poe, D. Gomez Martinez, T. Jian, N. J. Wolford, N. J. Jones, A. J. Ritz, R. A. Lazenby, J. K. Gibson, R. E. Baumbach, D. Páez-Hernández, M. L. Neidig, T. E. Albrecht-Schönzart, *Nat. Commun.* **2021**, *12*, 7230.
- [39] Nicholas A. Piro, J. R. Robinson, P. J. Walsh, E. J. Schelter, *Coord. Chem. Rev.* **2014**, *21*.
- [40] J.-C. Berthet, M. Nierlich, Y. Miquel, C. Madic, M. Ephritikhine, *Dalton Trans.* **2005**, 369.
- [41] D. D. Méndez-Hernández, P. Tarakeshwar, D. Gust, T. A. Moore, A. L. Moore, V. Mujica, *J. Mol. Model.* **2012**, *19*, 2845.
- [42] a) M. Namazian, C. Y. Lin, M. L. Coote, *J. Chem. Theory Comput.* **2010**, *6*, 2721; b) A. P. Davis, A. J. Fry, *J. Phys. Chem. A* **2010**, *114*, 12299.
- [43] R. D. Shannon, *Acta Cryst A* **1976**, *32*, 751.
- [44] F. Neese, *Wiley Interdiscip. Rev.: Comput. Mol. Sci.* **2012**, *2*, 73.
- [45] F. Neese, *Wiley Interdiscip. Rev.: Comput. Mol. Sci.* **2018**, *8*, e1327.
- [46] F. Neese, F. Wennmohs, U. Becker, C. Riplinger, *J. Chem. Phys.* **2020**, *152*, 224108.
- [47] H. J. V. Tyrrell, *Diffusion in Liquids. A Theoretical and Experimental Study*, Elsevier Science, Burlington, **1984**.
- [48] see Ref. [26].
- [49] a) I. Trapp, M. Löble, J. Meyer, F. Breher, *Inorg. Chim. Acta* **2011**, *374*, 373; b) M. W. Löble, M. Casimiro, D. T. Thielemann, P. Oña-Burgos, I. Fernández, P. W. Roesky, F. Breher, *Chem. Eur. J.* **2012**, *18*, 5325.
- [50] see Ref. [26].
- [51] I. Trapp, M. Löble, J. Meyer, F. Breher, *Inorg. Chim. Acta* **2011**, *374*, 373.
- [52] J. Koziskova, F. Hahn, J. Richter, J. Kožíšek, *Acta Chimica Slovaca* **2016**, *9*, 136.
- [53] O. V. Dolomanov, L. J. Bourhis, R. J. Gildea, J. A. K. Howard, H. Puschmann, *J. Appl. Crystallogr.* **2009**, *42*, 339.
- [54] G. M. Sheldrick, *Acta Crystallogr. Sect. A* **2015**, *71*, 3.
- [55] G. M. Sheldrick, *Acta Crystallogr. Sect. A* **2008**, *64*, 112.
- [56] G. M. Sheldrick, *Acta Crystallogr. Sect. C* **2015**, *71*, 3.
- [57] a) A. D. Becke, *Phys. Rev. A* **1988**, *38*, 3098–3100; b) J. P. Perdew, *Phys. Rev. B* **1986**, *33*, 8822.
- [58] F. Weigend, *Phys. Chem. Chem. Phys.* **2006**, *8*, 1057.
- [59] S. Grimme, J. Antony, S. Ehrlich, H. Krieg, *J. Chem. Phys.* **2010**, *132*, 154104.
- [60] J. Tao, J. P. Perdew, V. N. Staroverov, G. E. Scuseria, *Phys. Rev. Lett.* **2003**, *91*, 146401.
- [61] K. Eichkorn, F. Weigend, O. Treutler, R. Ahlrichs, *Theor. Chem. Acc.* **1997**, *97*, 119.
- [62] V. N. Staroverov, G. E. Scuseria, J. Tao, J. P. Perdew, *J. Chem. Phys.* **2003**, *119*, 12129.
- [63] F. Weigend, R. Ahlrichs, *Phys. Chem. Chem. Phys.* **2005**, *7*, 3297.
- [64] a) P. Erdmann, J. Leitner, J. Schwarz, L. Greb, *ChemPhysChem* **2020**, *21*, 987; b) H. Böhler, N. Trapp, D. Himmel, M. Schleep, I. Krossing, *Dalton Trans.* **2015**, *44*, 7489.
- [65] a) A. P. Davis, A. J. Fry, *J. Phys. Chem. A* **2010**, *114*, 12299; b) M. Namazian, C. Y. Lin, M. L. Coote, *J. Chem. Theory Comput.* **2010**, *6*, 2721.
- [66] a) see Ref. [37]; b) L. Lätsch, E. Lam, C. Copéret, *Chem. Sci.* **2020**, *11*, 6724–6735.

Manuscript received: May 15, 2023

Accepted manuscript online: June 9, 2023

Version of record online: July 24, 2023